Analysis of structural phase transitions by computer simulation

William C. Kerr
*Centre Européen de Calcul Atomique et Moléculaire, Université de Paris XI, Orsay, France and Department of Physics, Wake Forest University, Winston-Salem, North Carolina 27109**
(Received 19 October 1978)

This paper presents the results from molecular-dynamics calculations on a lattice-dynamical system which undergoes a structural phase transition. The characteristics of the model system used for the calculations are described in detail; the model is two dimensional, has an antiferrodistortive structural change, and is in the category of displacive structural transitions. The following results are obtained from the molecular-dynamics calculations. First, some equilibrium properties are shown, including the static correlation function, to establish that the system has a second-order phase transition. Second, the results for the time-dependent order parameter or soft-mode correlation function are given. Near the transition the spectral function for this correlation function exhibits a very narrow and intense central peak, in addition to the soft-mode peak. The temperature dependences of the soft-mode frequency and the central-peak width are given. The results obtained here are very similar to experimental observations, particularly on $SrTiO_3$, and they are used to argue that only intrinsic anharmonic mechanisms are needed to explain the origin of central peaks. Third, extensive results are given for the temperature and wave-vector dependence of the displacement correlation function, which give the wave-vector dependence of the central-peak characteristics. In a small temperature interval around the transition and in a small region of wave-vector space around but not including the soft-mode wave vector, the central peak is found to split so that the maximum is not exactly at zero frequency. Lastly, results for the energy-density correlation function are given for wave vectors around the soft-mode wave vector and for temperatures above the transition. Near the transition the corresponding spectral function is found to develop a pronounced high-frequency peak.

I. INTRODUCTION

The recognition that nonlinear interactions can produce phenomena which are qualitatively different from the situations occurring in the related linear systems is one achievement of much recent research in physics. Practically all areas of physics have been affected by this realization, and furthermore a rather small set of nonlinear equations has been found to describe a wide variety of physical systems and effects.[1]

Lattice dynamics is one established area of physics that has experienced new activity as a result of the discovery of the new effects which can result from nonlinearity. Traditionally, anharmonic lattice forces have been treated as weak perturbations to the linear forces, and on this basis, understanding of the finite lifetimes of lattice vibrations and of transport phenomena has been obtained.[2]

When the anharmonicity is not weak, one consequence can be that structural phase transitions occur. A mean-field type of perturbation theory for such transitions leading to the so-called "soft-mode" picture was proposed some years ago by Cochran[3,4] and by Anderson.[5] According to this picture, the frequency of one of the lattice modes goes to zero at the temperature of the structural transition and the static distortion of the lattice which occurs is described by the polarization vectors of that particular mode. Early experiments confirmed the correctness of this soft-mode theory.[6]

More recent experiments have shown that structural phase transitions are not adequately described by the mean-field theory. One such experiment is the measurement of the temperature dependence of the order parameter in strontium titanate[7] ($SrTiO_3$) showing that the value of the corresponding critical exponent is not that predicted by mean-field theory, but is consistent with the measured values for other second-order phase transitions, particularly magnetic and order-disorder systems. More closely related to the subject of this paper are measurements of the neutron scattering spectrum of $SrTiO_3$ by Riste *et al.*[8] and subsequently by Shapiro *et al.*[9,10] These measurements showed, in addition to the soft-mode peak, that there is a very intense and very narrow peak about zero frequency — the so-called "central peak". This central peak exists in a large temperature inter-

val about the transition, being observable at least 60 K above the transition temperature which is near 100 K in $SrTiO_3$. This interval is much wider than the 5-K interval below the transition in which the non-mean-field temperature dependence of the order parameter is observed.[7]

Since the original observation on $SrTiO_3$, central peaks have been observed in other crystals with the same lattice structure[9,11,12] ($KMnF_3$, $LaAlO_3$, $RbCaF_3$), in other insulating crystals[13] ($Pb_4Ge_3O_{11}$), in metals[14] (Nb_3Sn), in order-disorder systems[15] (KH_2PO_4), and in a molecular crystal[16] ($C_6Cl_4O_2$). Determination of the width of the central peak has not been possible in most of the neutron scattering experiments, since it has become narrower than the spectrometer resolutions. Recent high-resolution light scattering experiments on lead germanate[17] ($Pb_4Ge_3O_{11}$) using novel techniques, have measured the central-peak width to be about 5×10^{-6} eV full width at half maximum (FWHM). For $SrTiO_3$ indirect measurements from EPR data[18] and one high-resolution neutron scattering measurement[19] estimate the width to be about 0.5×10^{-6} eV. These experimental results have motivated considerable activity in search for the mechanism which produces such an extremely narrow peak.

Since the experimental observations from a wide variety of materials are so similar, the assumption has been widely made that they are a general result of anharmonicity, independent of any particular force law, and therefore simple models can be used for their analysis. Most theoretical work on this problem has been based on a Hamiltonian for an n-component continuum displacement field incorporating quartic anharmonic interactions, of the type made popular by renormalization-group theory. At least three different approaches can be distinguished in the work that has been done.

One approach, taken by Aubry,[20,21] and by Krumhansl and Schrieffer and their collaborators[22,23] has been to explore the consequences of the fact that the nonlinear equations of motion generated by this Hamiltonian have certain solutions which exist only by virtue of the nonlinearity. These solutions are antithetical to the familiar lattice wave solutions in that they are spatially localized whereas the lattice waves are spatially diffuse and are instead localized in wave-vector representation. Most but not all of this work has been on one-dimensional models where analytic derivations can be done in terms of elliptic functions and their limiting forms. These intrinsically nonlinear solutions take the form of propagating domain walls or cluster boundaries between large ordered regions of the crystal; the direction of ordering changes in passing through one of these walls. Nonrigorous but compelling arguments have been put forward by Aubry[21] and by Krumhansl and Schrieffer[22] that the motion of these domain walls is the cause of the central peak in the scattering spectra. The limitations on their arguments are the restriction to one dimension, where the only motion possible for a domain wall is simple propagation, and the consequent lack of a useful prediction for the temperature dependence of the intensity and width of the central peak in higher dimensions where the phase transition occurs at nonzero temperature.

A second theoretical approach to the central-peak problem has been to use the extension to dynamic critical phenomena[24] of the techniques of the renormalization group (RG).[25,26] The microscopic Hamiltonian for the structurally transforming system is assumed to be equivalent to the semiphenomenological "Model C" in a classification made by Halperin, Hohenberg, and Ma.[27] This is a model with a nonconserved order-parameter field coupled to an additional conserved field, which for this case is the energy density. A proof of this equivalence for a one-component order parameter has recently been given by Bausch and Halperin.[28] So far calculations of scattering lineshapes using the RG are based on the expansion in $4-d$,, where d is the dimensionality, and are strictly applicable only near four dimensions. Thus at the present time there is no close relation between this approach and the previously discussed approach,[21,22] which has achieved results only for low dimensionality. The RG calculations predict no central peak in the spectrum of the order-parameter fluctuations.[29]

The inability of these theories to give a central peak which is as narrow as the experimental observations has led to consideration of impurity mechanisms.[30,31] These theories conclude that a small concentration of impurities which couple to the order parameter can produce a sufficiently narrow central peak. In support of this position, electron paramagnetic resonance experiments have shown that impurities with the proper symmetry exist,[32] and purposeful enhancement of the impurity concentration in $SrTiO_3$ has been shown to increase the central-peak intensity.[33] These experiments show that impurities must certainly play a role in the dynamics producing the central peak, even though at the present time no definite impurity with a known coupling to the order-parameter fluctuations has been identified as the responsible agent.

The recent light scattering experiments on lead germanate by Fleury and Lyons[17] must be considered in conjunction with the results mentioned in the previous paragraph. These high-resolution experiments have identified two coexisting central peaks. One is so extremely narrow that it must be considered elastic and due to static impurities. The other is still very narrow compared to the soft phonon peaks and is attributed by these authors to an intrinsic anharmonic mechanism of the pure crystal. This experiment seems to indicate that the failure of current RG cal-

culations to find a central peak is not definitive and that impurities are not a necessary agent to have a central peak even though they are undoubtedly important in determining its characteristics, i.e., its intensity and width.

A third theoretical approach to understanding nonlinear systems which may improve understanding of these controversies, is the use of computer simulation or molecular dynamics. With this technique one-dimensional systems have been studied by Aubry,[21] Koehler *et al.*,[34] and Schneider and Stoll,[35] two-dimensional lattices by Schneider and Stoll,[36–40] by Bartolome and Kerr,[41] and by the present work, and three-dimensional lattices by Schneider and Stoll.[42] One advantage of the computer simulation studies is that the impurity content of the system can be precisely controlled. All simulation studies which have been reported up to the present time have been on completely pure systems; in all cases where the spectrum of the order-parameter fluctuations has been computed a central peak has been obtained.

This paper gives the results of a study of a two-dimensional lattice which exhibits a structural phase transition. The model differs in several important respects from that used in the other study of a two-dimensional system by Schneider and Stoll[36–40]; the differences are pointed out in the descriptions which follow. When this system is near its transition, the results for the spectral function for the order-parameter correlation function show a very intense and narrow central peak — so narrow that this result is used to argue that only intrinsic anharmonic mechanisms are necessary to explain most of the observed experimental results. In addition this work includes a more extensive analysis of the temperature and wave-vector dependence of the displacement correlation function than has been undertaken previously, and it presents results for the energy-density correlation function.

The outline of the paper is as follows. Sec. II describes the model used for the calculations, and Sec. III presents some of its properties. A brief discussion of some aspects of molecular-dynamics calculations is in Sec. IV. The results are presented in the following four sections: static properties in Sec. V, the order-parameter correlation function in Sec. VI, wave-vector-dependent displacement correlation function in Sec. VII, and energy-density correlation function in Sec. VIII. The conclusions are summarized in Sec. IX.

II. THE MODEL

In this section the model used for the calculations is described. This two-dimensional model has been constructed to be as simple as possible in the physical characteristics involved in the structural change; thus, it has a square lattice in both high- and low-temperature phases. In order to have simple dispersion relations for the lattice waves, the number of atoms per unit cell is as small as possible, namely, one atom per unit cell in the high-temperature phase and two atoms per cell in the low-temperature phase. In addition, the range of the interparticle forces is kept as short as possible, consistent with having the bare harmonic modes of the lattice stable throughout most of the Brillouin zone.

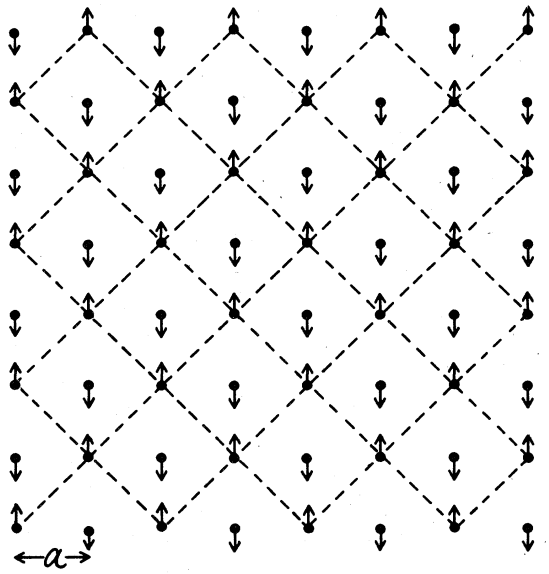

FIG. 1. Structure of the crystal lattice. The dots show the square structure of the high-temperature phase with lattice parameter a. The arrows show the displacement pattern of the unstable mode and the static displacements occurring at the transition. The dashed lines show the square structure of the low-temperature phase.

The structure of the high-temperature phase is square, as shown in Fig. 1. The lattice constant is a, and the two basis vectors of the structure are

$$\vec{a}_1 = a\,\vec{e}_1\,, \quad \vec{a}_2 = a\,\vec{e}_2\,, \tag{2.1}$$

where $\vec{e}_1$ and $\vec{e}_2$ are Cartesian unit vectors. The set of lattice vectors is given by

$$\vec{R} = l_x\,\vec{a}_1 + l_y\,\vec{a}_2\,, \tag{2.2}$$

where l_x and l_y are integers. The reciprocal lattice of the high-temperature phase is also square with basis vectors

$$\vec{g}_1 = (2\pi/a)\,\vec{e}_1\,, \quad \vec{g}_2 = (2\pi/a)\,\vec{e}_2\,. \tag{2.3}$$

The first Brillouin zone of the high-temperature lattice is the large outer square shown in Fig. 2.

The potential-energy function of the system is the sum of harmonic and anharmonic parts

$$\Phi = \Phi^{(h)} + \Phi^{(a)}\,. \tag{2.4}$$

The harmonic part $\Phi^{(h)}$ consists of pair interactions extending out to second nearest neighbors. Its explicit form is

$$\Phi^{(h)}=\tfrac{1}{2}M\omega_0^2\sum_{\vec{R}}\{\tfrac{1}{4}[u_x(\vec{R}+\vec{a}_1)-u_x(\vec{R})]^2+\tfrac{1}{4}(1+r_2-\bar{r}_4-g)[u_y(\vec{R}+\vec{a}_1)-u_y(\vec{R})]^2$$
$$+\tfrac{1}{4}(1+r_2-\bar{r}_4+g)[u_x(\vec{R}+\vec{a}_2)-u_x(\vec{R})]^2+\tfrac{1}{4}[u_y(\vec{R}+\vec{a}_2)-u_y(\vec{R})]^2$$
$$-\tfrac{1}{8}(1+r_2)\{[\bar{u}(\vec{R}+\vec{a}_1+\vec{a}_2)-\bar{u}(\vec{R})]^2+[\bar{u}(\vec{R}-\vec{a}_1+\vec{a}_2)-\bar{u}(\vec{R})]^2\}$$
$$+\tfrac{1}{4}r_5\{[u_x(\vec{R}+\vec{a}_1+\vec{a}_2)-u_x(\vec{R})][u_y(\vec{R}+\vec{a}_1+\vec{a}_2)-u_y(\vec{R})]$$
$$-[u_x(\vec{R}-\vec{a}_1+\vec{a}_2)-u_x(\vec{R})][u_y(\vec{R}-\vec{a}_1+\vec{a}_2)-u_y(\vec{R})]\}) \quad . \tag{2.5}$$

Here $u_\alpha(\vec{R})$, $\alpha=x,y$, denotes the αth component of the displacement of the particle associated with site $\vec{R}$ away from that lattice site. Each atom has two degrees of freedom; this is one of the major differences between this model and that of Schneider and Stoll,[40] which has a two-dimensional lattice but each atom has only one degree of freedom. M is the mass of a particle, ω_0 is a constant with the dimensions of frequency, so that $\frac{1}{4}M\omega_0^2$ is one of the nearest-neighbor harmonic force constants. The quantities r_2, $\bar{r}_4$, r_5, and g are all dimensionless constants.[43]

The harmonic part of the potential can be separated into a sum of single-particle terms $\Phi^{(hs)}$ and a sum of pair terms $\Phi^{(hp)}$, involving products of displacements at different sites, by multiplying out the brackets in Eq. (2.5). The single-particle part is

$$\Phi^{(hs)}=\tfrac{1}{2}M\omega_0^2\sum_{\vec{R}}[\tfrac{1}{2}(1-\bar{r}_4+g)u_x^2(\vec{R})$$
$$+\tfrac{1}{2}(1-\bar{r}_4-g)u_y^2(\vec{R})] \quad . \tag{2.6}$$

The classification of the structural change exhibited by the system as being either a displacive transition or an order-disorder transition is made essentially on the basis of the sign of the coefficients in this equation. If both coefficients are positive, then the transition is displacive. If one or both coefficients are negative, then the classification of the transition depends on the comparison of the thermal energy per particle at the transition to the depth of the well in the total (harmonic plus anharmonic) single-particle potential.[44] The coefficients are chosen so that this model has a displacive transition, as will be discussed in detail below.

The anharmonic part of the potential-energy function is

$$\Phi^{(a)}=\frac{1}{4}\left(\frac{M\omega_0^2}{a^2}\right)\sum_{\vec{R}}\{u_0[u_x^2(\vec{R})+u_y^2(\vec{R})]^2$$
$$+v_0[u_x^4(\vec{R})+u_y^4(\vec{R})]\} \quad . \tag{2.7}$$

Here u_0 and v_0 are additional dimensionless constants. This form of the anharmonic potential-energy function is taken from the renormalization-group analysis by Bruce and Aharony[45] of the possible phase diagrams of stressed perovskite crystals.

The force on the $\vec{R}$th particle obtained from the potential-energy function Φ also separates into harmonic and anharmonic parts,

$$\vec{F}(\vec{R})=\vec{F}^{(h)}(\vec{R})+\vec{F}^{(a)}(\vec{R}) \tag{2.8}$$

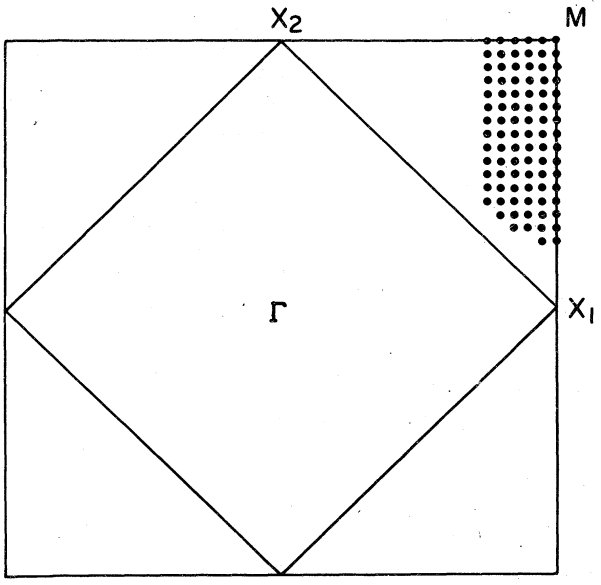

FIG. 2. Brillouin zones of the lattice. The outer and inner squares are the high- and low-temperature Brillouin zones, respectively. The dotted area is the region where the harmonic frequency $\omega_y^2(\vec{q})$ is negative.

and the explicit forms of these are as follows:

$$F_x^{(h)}(\vec{R}) = M\omega_0^2\{\tfrac{1}{4}[u_x(\vec{R}+\vec{a}_1)-2u_x(\vec{R})+u_x(\vec{R}-\vec{a}_1)]$$
$$+\tfrac{1}{4}(1+r_2-\bar{r}_4+g)[u_x(\vec{R}+\vec{a}_2)-2u_x(\vec{R})+u_x(\vec{R}-\vec{a}_2)]$$
$$-\tfrac{1}{8}(1+r_2)\,[u_x(\vec{R}+\vec{a}_1+\vec{a}_2)-2u_x(\vec{R})+u_x(\vec{R}-\vec{a}_1-\vec{a}_2)$$
$$+u_x(\vec{R}-\vec{a}_1+\vec{a}_2)-2u_x(\vec{R})+u_x(\vec{R}+\vec{a}_1-\vec{a}_2)]$$
$$+\tfrac{1}{8}r_5[u_y(\vec{R}+\vec{a}_1+\vec{a}_2)-2u_y(\vec{R})+u_y(\vec{R}-\vec{a}_1-\vec{a}_2)$$
$$-u_y(\vec{R}-\vec{a}_1+\vec{a}_2)+2u_y(\vec{R})-u_y(\vec{R}+\vec{a}_1-\vec{a}_2)]\}\ ; \tag{2.9}$$

$$F_y^{(h)}(\vec{R}) = M\omega_0^2\{\tfrac{1}{4}(1+r_2-\bar{r}_4-g)[u_y(\vec{R}+\vec{a}_1)-2u_y(\vec{R})+u_y(\vec{R}-\vec{a}_1)]$$
$$+\tfrac{1}{4}[u_y(\vec{R}+\vec{a}_2)-2u_y(\vec{R})+u_y(\vec{R}-\vec{a}_2)]$$
$$-\tfrac{1}{8}(1+r_2)[u_y(\vec{R}+\vec{a}_1+\vec{a}_2)-2u_y(\vec{R})+u_y(\vec{R}-\vec{a}_1-\vec{a}_2)$$
$$+u_y(\vec{R}-\vec{a}_1+\vec{a}_2)-2u_y(\vec{R})+u_y(\vec{R}+\vec{a}_1-\vec{a}_2)]$$
$$+\tfrac{1}{8}r_5[u_x(\vec{R}+\vec{a}_1+\vec{a}_2)-2u_x(\vec{R})+u_x(\vec{R}-\vec{a}_1-\vec{a}_2)$$
$$-u_x(\vec{R}-\vec{a}_1+\vec{a}_2)+2u_x(\vec{R})+u_x(\vec{R}+\vec{a}_1-\vec{a}_2)]\}\ ; \tag{2.10}$$

$$F_x^{(a)}(\vec{R}) = -(M\omega_0^2/a^2)\{u_0[u_x^2(\vec{R})+u_y^2(\vec{R})]u_x(\vec{R})+v_0u_x^3(\vec{R})\}\ , \tag{2.11}$$

$$F_y^{(a)}(\vec{R}) = -(M\omega_0^2/a^2)\{u_0[u_x^2(\vec{R})+u_y^2(\vec{R})]u_y(\vec{R})+v_0u_y^3(\vec{R})\}\ . \tag{2.12}$$

The quantities in square brackets in Eqs. (2.9) and (2.10) have the familiar form describing harmonic nearest-neighbor pair forces. In this case the harmonic force on the $\vec{R}$th particle comes from the four nearest neighbors at $\vec{R}\pm\vec{a}_1$, $\vec{R}\pm\vec{a}_2$, and the four next-nearest neighbors at $\vec{R}\pm\vec{a}_1\pm\vec{a}_2$. The terms in these equations proportional to r_5 couple the x and y components of the motions. Also, the harmonic force is seen to be translationally invariant. The anharmonic force is not translationally invariant; rather it restricts each particle to remain within a region around a lattice site fixed in space.

Although the lattice of the system has the point symmetry of a square, the harmonic potential energy $\Phi^{(h)}$ has only rectangular symmetry, as can be seen from the terms proportional to the parameter g in Eqs. (2.5), (2.6), (2.9), and (2.10). If $g=0$, then the potential-energy function has square symmetry. This anisotropy parameter is the same as the parameter g in the paper by Bruce and Aharony.[45] It describes the essential effects of the application of a uniaxial stress to the system. The most important effect for critical phenomena is to change the point symmetry of the lattice, which changes the universality class to which the system belongs and thus changes the critical exponents. The calculations reported here are for a single nonzero value of g. Important changes in the behavior of the system can be expected as a function of g, expecially near $g=0$. A qualitative discussion of these possibilities is given in Sec. III.

The mechanism causing the system to have a structural phase transition can be understood by analyzing the harmonic approximation for the system. Using only the harmonic forces of Eqs. (2.9) and (2.10), plane-wave solutions to the equations of motion are found in the standard fashion, and the squares of the frequencies of these lattice waves are obtained as the eigenvalues of the 2×2 dynamical matrix whose elements are

$$D_{xx}(\vec{q}) = \omega_0^2[2(1+r_2)\sin^2\tfrac{1}{2}q_xa\sin^2\tfrac{1}{2}q_ya - r_2\sin^2\tfrac{1}{2}q_xa-(\bar{r}_4-g)\sin^2\tfrac{1}{2}q_ya]\ , \tag{2.13}$$

$$D_{xy}(\vec{q}) = 2\omega_0^2r_5\sin\tfrac{1}{2}q_xa\cos\tfrac{1}{2}q_xa\sin\tfrac{1}{2}q_ya\cos\tfrac{1}{2}q_ya\ , \tag{2.14}$$

$$D_{yy}(\vec{q}) = \omega_0^2[2(1+r_2)\sin^2\tfrac{1}{2}q_xa\sin^2\tfrac{1}{2}q_ya - (\bar{r}_4+g)\sin^2\tfrac{1}{2}q_xa-r_2\sin^2\tfrac{1}{2}q_ya]\ . \tag{2.15}$$

For illustration, it can be seen that for wave vector $\vec{q}$ parallel to the x or y axes, the dispersion relations

have the same q dependence as the one-dimensional linear chain with nearest-neighbor forces.

In order to have a structural phase transition, there must be an unstable mode among the bare harmonic modes of the system, i.e., at least one of the vaues of ω^2 obtained from the dynamical matrix in Eqs. (2.13)–(2.15) must be negative. For the calculations reported here, the wave vector of the unstable mode is chosen to be at the Brillouin-zone corner

$$\vec{q}_c = (\pi/a)\,\vec{e}_1 + (\pi/a)\,\vec{e}_2 \,. \tag{2.16}$$

For the mode with this wave vector, the phase factor for the motion of the $\vec{R}$th particle is

$$e^{i\vec{q}_c\cdot\vec{R}} = (-1)^{l_x+l_y} \,, \tag{2.17}$$

so that adjacent atoms move in opposite directions. The arrows in Fig. 1 show one example of such a displacement pattern; other possibilities have the displacements parallel to some other direction. The dynamical matrix as given in Eqs. (2.13)–(2.15) is diagonal at $\vec{q}=\vec{q}_c$, so for that wave vector the modes are polarized parallel to the x and y axes. The squares of the corresponding frequencies are

$$\omega_x^2(\vec{q}_c) = \omega_0^2(2 + r_2 - \bar{r}_4 + g) \,, \tag{2.18}$$

$$\omega_y^2(\vec{q}_c) = \omega_0^2(2 + r_2 - \bar{r}_4 - g) \,. \tag{2.19}$$

The difference of these two quantities is proportional to the anisotropy parameter g; this nondegeneracy is a consequence of the rectangular symmetry of the potential-energy function.

The condition

$$2 + r_2 - \bar{r}_4 < 0 \tag{2.20}$$

is imposed on the parameters so that in the $g=0$ case with square symmetry the two (degenerate) modes at $\vec{q}_c$ are unstable. Then, for the calculations reported here, g is chosen to be positive and sufficiently large that $\omega_x^2(\vec{q}_c)$ is positive. This gives two additional conditions,

$$2 + r_2 - \bar{r}_4 + g > 0 \,, \tag{2.21}$$

$$2 + r_2 - \bar{r}_4 - g < 0 \,. \tag{2.22}$$

Thus only the mode with y polarization is unstable. The particle displacements occurring in this unstable mode are shown by the arrows in Fig. 1.

Additional restrictions are imposed on the parameters by requiring that all other modes are stable [except for a small region around $\vec{q}_c$ where $\omega_y^2(\vec{q}_c)$ must be negative by continuity], that longitudinal modes have higher frequencies than transverse modes, and that the number of accidental degeneracies of different branches of the dispersion relations be a minimum. These requirements lead to the conditions

$$r_2 < 0 \,, \tag{2.23}$$

$$\bar{r}_4 + g < 0 \,, \tag{2.24}$$

$$\bar{r}_4 - g < 0 \,, \tag{2.25}$$

$$-\bar{r}_4 - g < -r_2 \,, \tag{2.26}$$

$$-\bar{r}_4 + g < -r_2 \,, \tag{2.27}$$

$$0 < 4r_5 < (r_2 + \bar{r}_4)^2 - g^2 \,. \tag{2.28}$$

The set of parameters satisfying these conditions which has been used for the calculations is

$$r_2 = -2.7 \,, \tag{2.29}$$

$$\bar{r}_4 = -0.5 \,, \tag{2.30}$$

$$g = +0.4 \,, \tag{2.31}$$

$$r_5 = +0.5 \,. \tag{2.32}$$

With this choice of parameters both coefficients in Eq. (2.6) are positive, so this system undergoes a displacive transition. The bare harmonic dispersion relations resulting from these parameters are shown in Fig. 3 for selected directions in the Brillouin zone. The negative value of $\omega_y^2(\vec{q}_c)$ is evident in this figure. The region around $\vec{q}_c$ where $\omega_y^2(\vec{q})$ has negative values is shown by the dotted region of the Brillouin zone in Fig. 2. These modes are also unstable, but the mode at $\vec{q}_c$ determines the properties of the system because the absolute value $|\omega_y^2(\vec{q})|$ is largest at $\vec{q}=\vec{q}_c$ and this mode is thus the "most" unstable.

The anharmonic forces, whose specific form is derived from the potential in Eq. (2.7), stabilize the lattice against the instability of the harmonic forces. The structure of the low-temperature phase which results from the interplay of these two forces is most easily obtained at zero temperature by finding the configuration which minimizes the total potential energy $\Phi = \Phi^{(h)} + \Phi^{(a)}$. The displacements of the atoms in the unstable mode with wave vector $\vec{q}_c$ have no x component, and the y component is

$$u_y(\vec{R}) = (-1)^{l_x+l_y} S \,, \tag{2.33}$$

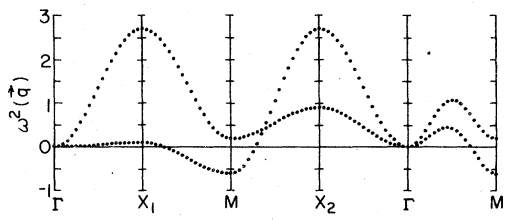

FIG. 3. Square of the bare harmonic lattice frequencies plotted for selected directions in the Brillouin zone. The labels of the vertical axes correspond to the labelled points in Fig. 2. The dots are placed at the allowed wave vectors for a 40×40 lattice with periodic boundary conditions.

where S is the constant magnitude of the atomic displacements in this mode. For this particular displacement pattern, the total potential energy per particle is

$$\frac{\Phi}{N}=\frac{1}{2}M\omega_0^2(2+r_2-\bar{r}_4-g)S^2 + \frac{1}{4}\left[\frac{M\omega_0^2}{a^2}\right](u_0+v_0)S^4 . \quad (2.34)$$

For global stability of the system, this equation shows that u_0+v_0 must be positive. The coefficient of the quadratic term is negative, as shown by Eq. (2.22), so that the potential energy in configuration space along the direction specified by Eq. (2.33) has a double-well shape.

The magnitude of the static displacements occurring at zero temperature is given by

$$S^2=-[(2+r_2-\bar{r}_4-g)/(u_0+v_0)]a^2 , \quad (2.35)$$

which is obtained by minimizing Φ in Eq. (2.34), Thus the atoms shift by a finite amount up and down parallel to the y axis, producing an antiferrodistortive structural transition. The resulting crystal structure is shown by the dotted lines in Fig. 1. This structure is also a square structure, but the primitive unit cell contains two atoms, and it has twice the area of the high-temperature unit cell. The first Brillouin zone of the low-temperature structure is shown by the inner square in Fig. 2. From Fig. 2 it is evident that the wave vector $\vec{q}_c$ of the soft mode, which is at the corner of the Brillouin zone of the high-temperature phase, becomes a zone-center point in the low-temperature phase.

For the calculations presented in this paper, the two parameters of the anharmonic interaction have been given the values

$$u_0=30 , \quad v_0=-10 . \quad (2.36)$$

From the values of the parameters of the harmonic potential energy in Eqs. (2.29)–(2.32) and from Eq. (2.36), the magnitude of the static displacement of the particles at zero temperature is obtained from Eq. (2.35) to be

$$S/a=(0.03)^{1/2}=0.173 , \quad (2.37)$$

and the minimum potential energy per particle is obtained from Eqs. (2.34) and (2.35) to be

$$\Phi_{\min}/NM\omega_0^2a^2=-4.5\times10^{-3} . \quad (2.38)$$

III. CHARACTERISTICS OF THE MODEL

Two properties of the model introduced in Sec. II are presented here. First, the possible phase diagrams of the system in the plane defined by the anisotropy parameter g and the temperature T are described using mean-field theory. This is included in order to illustrate the different possibilities contained in the model, even though it is known that mean-field theory does not give an accurate description of phase transitions. Secondly, the nonlinear equations of motion which describe the system in the continuum approximation are given.

A. Mean-field approximation

The derivation of the mean-field theory for this model closely follows that given by Thomas[46] for a one-dimensional case. Since the form of the anharmonic potential is the same as that used by Bruce and Aharony,[45] the results obtained here are very similar to theirs.

The mean-field theory first calculates the properties of the single-particle system defined by the potential-energy function

$$\Phi_{\vec{R}}=\tfrac{1}{2}M\omega_0^2[\tfrac{1}{2}(1-\bar{r}_4+g)u_x^2+\tfrac{1}{2}(1-\bar{r}_4-g)u_y^2]+\tfrac{1}{4}(M\omega_0^2/a^2)[u_0(u_x^2+u_y^2)^2+v_0(u_x^4+u_y^4)]-\vec{F}^{\,\mathrm{ext}}\cdot\vec{u} . \quad (3.1)$$

The harmonic and anharmonic single-particle potential energies in Eq. (3.1) are the terms from Eqs. (2.6) and (2.7), respectively, which refer only to atom $\vec{R}$; the last term is the interaction with an external force. The thermodynamic and response functions of this single-particle system are calculated by assuming a single-particle density distribution of the form appropriate for a harmonic oscillator[46]

$$\rho(\vec{u})=\frac{e^{-(u_x-U_x)^2/2\sigma_x}}{(2\pi\sigma_x)^{1/2}}\frac{e^{-(u_y-U_y)^2/2\pi\sigma_y}}{(2\pi\sigma_y)^{1/2}} , \quad (3.2)$$

in which the parameters U_α, σ_α, $\alpha=x$, and y are determined by minimizing the single-particle free energy. This *Ansatz* assumes that the single-particle density contours have elliptical shape and that the principal axes of the contours remain parallel to the coordinate axes. This assumption is justified by the rectangular symmetry of the model. Using Eq. (3.2) gives the expectation value of the configurational energy as

$$E=\tfrac{1}{2}M\omega_0^2[\tfrac{1}{2}(1-\bar{r}_4+g)(U_x^2+\sigma_x)+\tfrac{1}{2}(1-\bar{r}_4-g)(U_y^2+\sigma_y)] + \tfrac{1}{4}(M\omega_0^2/a^2)\{(u_0+v_0)[(U_x^4+6U_x^2\sigma_x+3\sigma_x^2)+(U_y^4+6U_y^2\sigma_y+3\sigma_y^2)]+2u_0(U_x^2+\sigma_x)(U_y^2+\sigma_y)\} , \quad (3.3)$$

and of the configurational entropy as

$$S = -k_B \langle \ln\rho \rangle = k_B + \tfrac{1}{2}k_B \ln(2\pi\sigma_x) + \tfrac{1}{2}k_B \ln(2\pi\sigma_y) \ . \tag{3.4}$$

The four parameters U_α, σ_α, $\alpha = x$, and y, are chosen to minimize the free energy $E - TS$ (T is the temperature) and are the solutions of the four equations

$$M\omega_0^2 U_x \{\tfrac{1}{2}(1-\bar{r}_4+g) + a^{-2}[(u_0+v_0)(U_x^2+3\sigma_x) + u_0(U_y^2+\sigma_y)]\} = F_x^{\text{ext}} \ , \tag{3.5}$$

$$M\omega_0^2 U_y \{\tfrac{1}{2}(1-\bar{r}_4-g) + a^{-2}[(u_0+v_0)(U_y^2+3\sigma_y) + u_0(U_x^2+\sigma_x)]\} = F_y^{\text{ext}} \ , \tag{3.6}$$

$$M\omega_0^2 \sigma_x \{\tfrac{1}{2}(1-\bar{r}_4+g) + a^{-2}[3(u_0+v_0)(U_x^2+\sigma_x) + u_0(U_y^2+\sigma_y)]\} = k_B T \ , \tag{3.7}$$

$$M\omega_0^2 \sigma_y \{\tfrac{1}{2}(1-\bar{r}_4-g) + a^{-2}[3(u_0+v_0)(U_y^2+\sigma_y) + u_0(U_x^2+\sigma_x)]\} = k_B T \ . \tag{3.8}$$

In mean-field theory the effects of the interparticle interaction are accounted for by including as part of the total force acting on the $\vec{R}$th particle, the interparticle forces from the neighbors of that particle evaluated at the mean position $\vec{U}(\vec{R})$ for those particles. That is, in Eqs. (3.5) and (3.6), the following replacements are made:

$$F_\alpha^{\text{ext}} \rightarrow F_\alpha^{\text{ext}}(\vec{R}) + \sum_{\substack{\vec{R}',\alpha' \\ \vec{R}' \neq R}} \Gamma_{\alpha\alpha'}(\vec{R}-\vec{R}')U_{\alpha'}(\vec{R}') \ ,$$

$$\alpha, \alpha' = x,y \ . \tag{3.9}$$

The force constants $\Gamma_{\alpha\alpha'}(\vec{R})$ which are nonzero may be found by inspection from the potential-energy function $\Phi^{(h)}$ in Eq. (2.5) and are listed in Table I.

To determine the values of the parameters where a phase transition occurs, solutions of Eqs. (3.5)–(3.9) must be found with $\vec{U}(\vec{R}) \neq 0$ but with $\vec{F}^{\text{ext}}(\vec{R}) = 0$. To do this, the fact from Sec. II that the soft mode has wave vector $\vec{q}_c$ is used, and therefore the static displacements occurring at the transition have the spatial dependence

$$\vec{U}(\vec{R}) = (-1)^{l_x+l_y}\vec{S} \ , \tag{3.10}$$

where $\vec{S}$ is independent of position and is the order parameter for the transition. When Eq. (3.10) is substituted into Eqs. (3.5)–(3.9), then Eqs. (3.5) and (3.6) become

$$M\omega_0^2 \{(2+r_2-\bar{r}_4+g) + a^{-2}[(u_0+v_0)(S_x^2+3\sigma_x) + u_0(S_y^2+\sigma_y)]\}S_x = 0 \ , \tag{3.11}$$

$$M\omega_0^2 \{(2+r_2-\bar{r}_4-g) + a^{-2}[(u_0+v_0)(S_y^2+3\sigma_y) + u_0(S_x^2+\sigma_x)]\}S_y = 0 \ . \tag{3.12}$$

Equations (3.7) and (3.8) remain the same except for the replacement of U_α by S_α. To get Eqs. (3.11) and (3.12) the relations

$$\sum_{\substack{\vec{R} \\ \vec{R} \neq 0}} \Gamma_{\alpha\alpha'}(\vec{R})(-1)^{l_x+l_y} = \begin{cases} -M\omega_0^2(3+2r_2-\bar{r}_4+g) \ , & \alpha = \alpha' = x \ , \\ 0 \ , \quad \alpha = x \ , \quad \alpha' = y \ , & \\ -M\omega_0^2(3+2r_2-\bar{r}_4-g) \ , & \alpha = \alpha' = y \end{cases} \tag{3.13}$$

obtained from Table I, have been used.

To solve Eqs. (3.7), (3.8), (3.11), and (3.12), the polar representation of the order parameter

$$S_x = S\cos\theta \ , \quad S_y = S\sin\theta \ , \tag{3.14}$$

and the auxiliary quantities

$$\sigma = \sigma_x + \sigma_y \ , \quad \Delta\sigma = \sigma_x - \sigma_y \ , \tag{3.15}$$

TABLE I. Harmonic force constants used for calculating the mean force in Sec. III and for calculating the energy density in Sec. VIII.

$\vec{R}$	$\alpha\beta$	$\Gamma_{\alpha\beta}(\vec{R})$
$\pm\vec{a}_1$	xx	$\frac{1}{4}$
	yy	$\frac{1}{4}(1+r_2-\bar{r}_4-g)$
$\pm\vec{a}_2$	xx	$\frac{1}{4}(1+r_2-\bar{r}_4+g)$
	yy	$\frac{1}{4}$
$\pm(\vec{a}_1+\vec{a}_2)$	xx,yy	$-\frac{1}{8}(1+r_2)$
	xy,yx	$\frac{1}{8}r_5$
$\pm(-\vec{a}_1+\vec{a}_2)$	xx,yy	$-\frac{1}{8}(1+r_2)$
	xy,yx	$-\frac{1}{8}r_5$

are convenient to use. In terms of these variables the four equations to be solved are

$$S\sin2\theta[2g+(2u_0+3v_0)a^{-2}\Delta\sigma+v_0a^{-2}S^2\cos2\theta]=0\ , \tag{3.16}$$

$$S^2[(2+r_2-\bar{r}_4)+g\cos2\theta+\tfrac{1}{2}(4u_0+3v_0)a^{-2}\sigma+\tfrac{1}{2}(2u_0+3v_0)a^{-2}\Delta\sigma\cos2\theta+u_0a^{-2}S^2+\tfrac{1}{2}v_0a^{-2}S^2(1+\cos^2 2\theta)]=0\ , \tag{3.17}$$

$$\tfrac{1}{2}(1-\bar{r}_4)a^{-2}\sigma+\tfrac{1}{2}ga^{-2}\Delta\sigma+\tfrac{3}{2}(u_0+v_0)a^{-4}S^2(\sigma+\Delta\sigma\cos2\theta)+\tfrac{1}{2}u_0a^{-4}S^2(\sigma-\Delta\sigma\cos2\theta)$$
$$+\tfrac{3}{2}(u_0+v_0)a^{-4}[\sigma^2+(\Delta\sigma)^2]+\tfrac{1}{2}u_0a^{-4}[\sigma^2-(\Delta\sigma)^2]=2k_BT/M\omega_0^2a^2\ , \tag{3.18}$$

$$\tfrac{1}{2}(1-\bar{r}_4)a^{-2}\Delta\sigma+\tfrac{1}{2}ga^{-2}\sigma+\tfrac{3}{2}(u_0+v_0)a^{-4}\sigma\Delta\sigma+\tfrac{3}{2}(u_0+v_0)a^{-4}S^2(\Delta\sigma+\sigma\cos2\theta)+\tfrac{1}{2}u_0a^{-4}S^2(\Delta\sigma-\sigma\cos2\theta)=0\ . \tag{3.19}$$

To solve these equations, use is made of the knowledge from Sec. II that for the case of a positive anisotropy parameter $g>0$, the soft mode is polarized parallel to the y axis, whereas for $g<0$ it is polarized parallel to the x axis. Thus, for the solution of Eq. (3.16), the appropriate root is

$$\sin2\theta=0\ ,\quad \begin{matrix}\theta=\pi/2\ ,\ g>0\\ \theta=0\ ,\ g<0\end{matrix}\ . \tag{3.20}$$

For the case $g>0$, Eq. (3.17) can be solved for the order parameter

$$a^{-2}S^2=[-(2+r_2-\bar{r}_4-g)-\tfrac{1}{2}(4u_0+3v_0)a^{-2}\sigma$$
$$+\tfrac{1}{2}(2u_0+3v_0)a^{-2}\Delta\sigma]/(u_0+v_0)\ . \tag{3.21}$$

For this solution to be physically possible, the numerator must be positive; thus the condition defining the phase boundary is

$$(4u_0+3v_0)a^{-2}\sigma_c-(2u_0+3v_0)a^{-2}\Delta\sigma_c$$
$$=-2(2+r_2-\bar{r}_4-g)\ . \tag{3.22}$$

The other relation between σ and $\Delta\sigma$ is Eq. (3.19), which becomes, on the phase boundary,

$$\tfrac{1}{2}(1-\bar{r}_4)a^{-2}\Delta\sigma_c+\tfrac{1}{2}ga^{-2}\sigma_c+3(u_0+v_0)a^{-4}\sigma_c\Delta\sigma_c=0\ . \tag{3.23}$$

The mean-field transition temperature is obtained by substituting the solution of Eqs. (3.22) and (3.23) into Eq. (3.18) with $S=0$,

$$\frac{2k_BT_c}{M\omega_0^2a^2}=\tfrac{1}{2}(1-\bar{r}_4)a^{-2}\sigma_c+\tfrac{1}{2}ga^{-2}\Delta\sigma_c$$
$$+\tfrac{3}{2}(u_0+v_0)a^{-4}[\sigma_c^2+(\Delta\sigma_c)^2]$$
$$+\tfrac{1}{2}u_0a^{-4}[\sigma_c^2-(\Delta\sigma_c)^2]\ . \tag{3.24}$$

A similar set of equations can be derived for the $g<0$ case.

Substituting the values of the parameters from Eqs. (2.29)–(2.32) and (2.36) *except* for g, Eqs. (3.22)–(3.24) (and the corresponding set for $g<0$) can be solved to give the transition temperature T_c as a function of the anisotropy parameter g; the results are shown in Fig. 4. This phase diagram is very similar to that in Fig. 2 of Ref. 45. For $g>0$ the ordering is parallel to the y axis, and for $g<0$ it is parallel to the x axis. There is a discontinuous change in the ordering direction where g changes sign, so the portion of the $g=0$ axis out to the intersection of the two phase boundaries is a "flop line". The point where the flop line and the two phase boundaries intersect is a "bicritical point".

At $g=0.4$, which is the value used for the molecular-dynamics calculations, the mean-field transition temperature is $8.312\times10^{-3}M\omega_0^2a^2/k_B$.

For nonzero g values, the system is in the same universality class as the two-dimensional Ising model. For $g=0$, the system is still anisotropic with square symmetry due to the v_0 term in the anharmonic potential, and it is then in the same universality class as one of the models studied by Schneider and Stoll.[47] If the parameter v_0 is set to zero, then this model be-

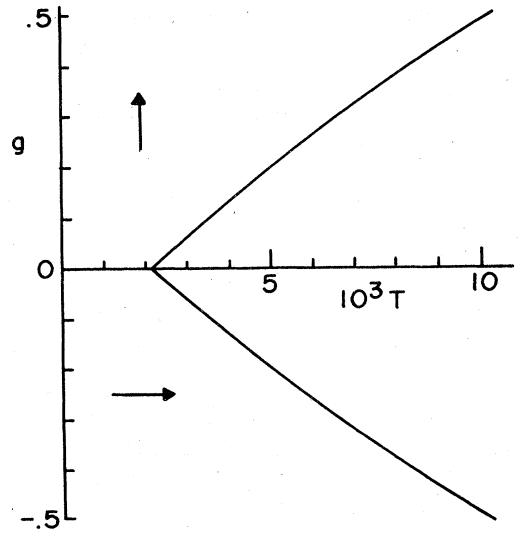

FIG. 4. Phase diagram in the anisotropy-parameter–temperature plane. The arrows show the direction in which ordering occurs for positive and negative values of g, respectively.

comes equivalent to the two-dimensional XY model, for which it is well known there is no phase transition with long-range order.[48] The XY model in two dimensions evidently has a phase transition involving a divergence of the susceptibility below some critical temperature but no long-range order.[49,50] So far, though, no numerical work has been done with this model to study the crossover either to the $g=0$ square symmetry case or to the $v_0=0$ isotropic case.

The mean-field theory outlined here would give yet another solution by setting the expression in brackets in Eq. (3.16) to zero. This solution would have the angle θ change continuously with g and would have a phase diagram in mean-field theory like Fig. 3 of Ref. 45, with a tetracritical point. According to Ref. 45 this would be the chosen solution if the parameter v_0 were positive rather than negative. This parameter has been chosen negative here in order to do the molecular-dynamics calculations for the simpler of the two possibilities.

This discussion shows that there is considerable variety available in the model concerning the type of ordering that occurs in the low-temperature phase. The calculations presented here are for a single, negative value for v_0 and a single, positive value for g.

B. Continuum equations of motion

The model system orders by taking on a static displacement pattern which alternates in direction in going from one atom to any of its nearest neighbors, as shown in Sec. II. This displacement pattern varies rapidly on the scale of interatomic distances, and thus the displacement field is not the proper function to use in a continuum description of the system near the transition. Instead the proper function to use is the (dimensionless) staggered displacement field $\vec{S}(\vec{R}, t)$, defined by reversing the displacement on alternate lattice sites,

$$a\vec{S}(\vec{R}, t) = (-1)^{l_x+l_y}\vec{u}(\vec{R}, t) . \tag{3.25}$$

The first factor on the right-hand side of Eq. (3.25) eliminates the rapid alternations of the displacement field.

Near the transition the system is expected to break up into ordered regions where $\vec{S}(\vec{R}, t)$ is spatially practically constant, separated by boundaries through which $\vec{S}(\vec{R}, t)$ changes sign. Because the parameters of the potential-energy function are appropriate for a displacive transition, these boundary regions are several lattice constants wide. Thus, near the transition the staggered displacement field varies slowly on the interatomic scale, and writing continuum equations for this quantity is appropriate.

The derivation of the continuum equations of motion is straightforward so the details will be omitted. The equations of motion obtained from the force expressions in Eqs. (2.9)–(2.12) are first rewritten in terms of the staggered displacement field. Then it is assumed that the site variable $\vec{R}$ can be treated as a continuous variable $\vec{r}$ and that at any of the neighbor sites $\vec{r}+\vec{\delta}$ of the position $\vec{r}$, $S_\alpha(\vec{r}+\vec{\delta})$ can be expressed in terms of $S_\alpha(\vec{r})$ by a Taylor expansion,

$$S_\alpha(\vec{r}+\vec{\delta}) = S_\alpha(\vec{r}) + \sum_\mu \delta_\mu \nabla_\mu S_\alpha(\vec{r}) + \frac{1}{2}\sum_{\mu,\nu}\delta_\mu\delta_\nu\nabla^2_{\mu\nu}S_\alpha(\vec{r}) + \cdots , \tag{3.26}$$

where $\nabla_\mu \equiv \partial/\partial r_\mu$. The following coupled nonlinear partial differential equations are then obtained for the components of $\vec{S}(\vec{r}, t)$:

$$\frac{\partial^2 S_x}{\partial t^2} - \omega_0^2 a^2\left[-\tfrac{1}{4}(2+r_2-\bar{r}_4) - \tfrac{1}{8}(r_2+\bar{r}_4)\right]\nabla^2 S_x + \omega_0^2(2+r_2-\bar{r}_4+g)S_x$$
$$-\tfrac{1}{8}\omega_0^2 a^2(r_2-\bar{r}_4)(\nabla_x^2 S_x - \nabla_y^2 S_x) + \omega_0^2 a^2 g\nabla_y^2 S_x - \omega_0^2 a^2 r_5 \nabla_{xy}^2 S_y + \omega_0^2[u_0(S_x^2+S_y^2)S_x + v_0 S_x^3] = 0 , \tag{3.27}$$

$$\frac{\partial^2 S_y}{\partial t^2} - \omega_0^2 a^2\left[-\tfrac{1}{4}(2+r_2-\bar{r}_4) - \tfrac{1}{8}(r_2+\bar{r}_4)\right]\nabla^2 S_y + \omega_0^2(2+r_2-\bar{r}_4-g)S_y$$
$$-\tfrac{1}{8}\omega_0^2 a^2(r_2-\bar{r}_4)(\nabla_x^2 S_y - \nabla_y^2 S_y) - \omega_0^2 a^2 g\nabla_x^2 S_y - \omega_0^2 a^2 r_5 \nabla_{xy}^2 S_x + \omega_0^2[u_0(S_x^2+S_y^2)S_y + v_0 S_y^3] = 0 . \tag{3.28}$$

The origin of the terms in these equations can be readily identified. The first three terms form the familiar Klein-Gordon (KG) equation. The coefficient of the Laplacian is positive by the inequalities in Eqs. (2.20)– (2.28). The third term (the "mass-squared" term of the KG equation) enters because the harmonic part of the Hamiltonian does not remain invariant under a uniform staggered displacement field, as it does for a uniform displacement field. The coefficient of the third term in the equation for S_x is positive [cf. Eq. (2.21)] because that mode is stable, whereas the coefficient of the third term in the equation for S_y is negative [cf. Eq. (2.22)] describing the instability of that mode in the harmonic approximation. The remaining linear terms of these two equations describe the reduced sym-

metry of this lattice system. The KG terms are isotropic; the reduction to square symmetry is described by the fourth term. The further reduction of the symmetry to rectangular is described by the fifth term, proportional to the anisotropy parameter g. The sixth term gives the coupling between the x and y components. Finally, the last terms describe the nonlinear forces.

Coupled nonlinear partial differential equations such as these have been studied very little. Some references to work on similar equations are given in a recent review article by Makhankov.[51]

For simple situations, the equations reduce to more familiar forms. For example, if attention is restricted to motions which have only a y component and depend only on the y coordinate, then the equations reduce to

$$\frac{\partial^2 S_y}{\partial t^2}+\frac{1}{4}\omega_0^2 a^2(2+2r_2-\bar{r}_4)\nabla_y^2 S_y + \omega_0^2(2+r_2-\bar{r}_4-g)S_y+\omega_0^2(u_0+v_0)S_y^3=0 \ . \quad (3.29)$$

This equation is essentially identical to the ones studied by Krumhansl and Schrieffer[22] and by Aubry,[21] including having the same signs for the coefficients. [There is a similar equation describing motions parallel to the x axis, but in that equation the coefficient of the linear term is positive, using the condition on the model expressed in Eq. (2.21), and its solutions are not so interesting.] Thus, the domain wall solutions discussed at length by Krumhansl and Schrieffer and by Aubry are among the motions of this lattice. Presumably there are also other more complicated, intrisically nonlinear solutions of the Eqs. (3.27) and (3.28).

IV. MOLECULAR-DYNAMICS CALCULATIONS

Some of the details of the molecular-dynamics (MD) method used to obtain information about the model system are given in this section.

The MD method is the numerical solution of the classical equations of motion for the positions and velocities of all the particles for a system containing a relatively small number of particles interacting through the forces of the model. This solution is the phase-space trajectory of the system, and by suitable averaging over this trajectory thermodynamic functions and correlation functions can be calculated. The method was first used for fluids with hard-sphere interactions by Alder and Wainwright,[52] extended to liquids with continuous potentials by Rahman,[53] and since then has been used successfully to study many other situations including plasmas, molten salts, lattice vibrations, superionic conductors, etc. In principle the method gives the most detailed information that can be obtained for a classical system. The limitations of the method are that the finite difference techniques used to integrate the equations generate numerical inaccuracies and that computer limitations restrict both the number of particles which can be used and the time interval over which the solution can be obtained, and thus there are difficulties obtaining adequate statistics for the averages. Furthermore the force law for the system to be studied is usually not known exactly, and approximate representations of the forces must be used for the calculations.

The calculations presented here are for a system of 1600 particles arranged on a 40×40 lattice with periodic boundary conditions. An integration algorithm developed by Beeman[54] was employed because it allows the use of a long time step while still maintaining good accuracy in the solution. Beeman's algorithm has been shown to be closely related to another one developed by Verlet[55,56] which has been extensively used.

Information concerning the several MD runs made for these calculations is given in Table II. For most of the runs the time-step Δt used for the integration was 0.3 in units of ω_0^{-1}, where ω_0 is the parameter with dimensions of angular frequency appearing in the potential-energy function in Eq. (2.5). With this time step the total energy oscillated very slightly about a mean value; these mean values (in units of $M\omega_0^2 a^2$) and the corresponding relative root-mean-square deviations are shown in Table II. At the two lowest energies where the particles are moving more slowly, Δt was increased to 0.4, which caused the

TABLE II. Information concerning the molecular-dynamics runs. Δt is the time step in units of ω_0^{-1}, N_t is the number of time steps calculated, E/N is the energy per particle in units of $M\omega_0^2 a^2$, and ΔE is the rms deviation in the energy.

Δt (ω_0^{-1})	N_t	$(E/N)\times 10^3$ ($M\omega_0^2 a^2$)	$(\Delta E/E)\times 10^2$
0.3	36 000	20.880	0.040
0.3	36 000	16.006	0.039
0.3	12 600	12.055	0.043
0.3	36 000	10.386	0.054
0.3	56 000	9.662	0.066
0.3	36 000	9.263	0.072
0.3	36 600	8.911	0.081
0.3	36 000	8.569	0.081
0.4	36 000	7.205	0.141
0.4	36 000	6.533	0.147

variation in total energy to increase. These values of Δt are on the order of $\frac{1}{10}$ of the period of the highest-frequency vibrational mode of the lattice. This is rather longer than the time interval used by Schneider and Stoll,[36] who state that they have 70 time steps in each period of the highest-frequency vibration. Being able to use a time step longer is an advantage since it means that more of the phase space has been sampled for a given amount of computing effort and thus more statistically independent configurations are available to compute averages.

Table II also shows the total length of each of the MD runs in terms of the number of time steps Δt. These runs were all taken after the system was allowed to "age" for a considerable time in order to eliminate effects of the rather special initial conditions used to start the calculations.

Once the positions and velocities of all the particles are known as functions of time, the average values of dynamical variables which depend on these positions and velocities are computed by the formula

$$\langle A \rangle = N_c^{-1} \sum_{j=1}^{N_c} A(\tau_j) \tag{4.1}$$

and correlation functions are computed from

$$\langle A(t)A(0) \rangle = \langle A(t+\tau)A(\tau) \rangle = N_c^{-1} \sum_{j=1}^{N_c} A(t+\tau_j)A(\tau_j) \ . \tag{4.2}$$

N_c denotes the number of different phase-space configurations used in the sums.

Special problems arise when the MD method is used to study systems which have a phase transition.[57] These arise because finite systems with periodic boundary conditions can not have phase transitions. A particularly graphic discussion of this fact has been given by Gallavoti.[58] The problem may be understood by considering the temporal behavior of the instantaneous order parameter $P(t)$ which for this system is the average of the staggered displacement field, defined in Eq. (3.25), averaged over all the lattice sites $\vec{R}$ [see Eq. (5.2) in Sec. V]. At high temperatures the system point in phase space moves back and forth between regions of phase space in which $P(t)$ has opposite signs many times in the course of one MD run. The average value $\langle P \rangle$ is approximately zero, and averages calculated over this run give a good description of the high-temperature phase. At low temperatures, since the finite system has no phase transition, the phase-space point must continue to move between regions where $P(t)$ has opposite signs, but the time interval between sign changes becomes very long. The MD run can then be entirely contained within a time interval where the phase-space point stays in the region of phase space where $P(t)$ has a constant sign. It is assumed that averages over this finite MD run give good approximations for the order parameter and other properties of the infinite system in the low-temperature phase. All MD calculations on the ordered phase of systems having a phase transition must be interpreted in this way. Furthermore, there must be a temperature interval around T_c of the infinite system in which MD calculations can not give reliable information. In this interval the phase-space point makes a small number of transitions between regions in which $P(t)$ has opposite signs, so the results can not describe the low-temperature phase, but not enough of these transitions are made to give an adequate sampling of the phase space for the high-temperature phase. The size of this temperature interval is decreased by increasing the number of particles in the system.

TABLE III. Units.

Quantity	Unit
Length	a
Time	ω_0^{-1}
Mass	M
Frequency	ω_0
Force	$M\omega_0^2 a$
Energy	$M\omega_0^2 a^2$
Temperature	$M\omega_0^2 a^2/k_B$
Specific heat	k_B
Susceptibility	$1/M\omega_0^2$

As the last item in this section, the units for the calculation and presentation of the results are introduced. All calculations are done in dimensionless form, with all lengths expressed in terms of the lattice constant a, and time in units of ω_0^{-1}, where ω_0 is the parameter in the potential-energy function in Eq. (2.5). There is only one mass M for all the particles so this is used for the mass unit. The units of some other quantities are given in Table III. All of the results in Secs. V–IX are presented in terms of these units.

V. STATIC QUANTITIES

This section contains the results for the static thermodynamic properties of the system. The results for quantities which integrate over all the modes of the system are presented first, followed by those quantities which are more sensitive to the mode directly involved in the transition.

All of the results here and in Secs. VI–IX are given in terms of the dimensionless units described in Sec. IV.

The total energy of the system as a function of the temperature is shown by the points in Fig. 5(a). The solid line shows the energy of a harmonic system (with a specific heat per particle equal to two) which has the same energy at zero temperature. The harmonic contributions are seen to be the major part of the total energy. Also, the total energy is positive at all the temperatures for which calculations were done, including points both above and below the transition. Thus even in the ordered phase the system can have sufficient energy that if it were all concentrated in the soft mode, the system could cross over the potential barrier in configuration space [cf. Eq. (2.34)]. Both of these properties are characteristic of displacive transitions. It should be recalled from Sec. II that this system has a displacive transition because each single-particle potential has a minimum at the lattice site and the transition is driven by the elastic interaction energy.

Figure 5(b) shows just the anharmonic energy versus temperature. It rises sharply from zero at zero temperature, passes through a maximum, and then declines more slowly. The derivative of this function is the excess specific heat above the harmonic value. The derivative becomes largest at a temperature slightly less than 6×10^{-3}, indicating that a phase transition takes place near that temperature.

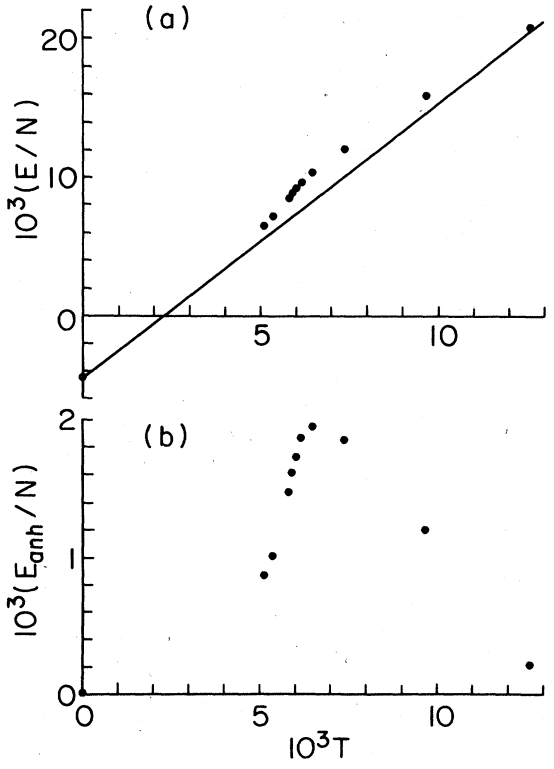

FIG. 5. Energy vs temperature. (a) shows the total energy, and (b) shows only the anharmonic part.

The specific heat can be obtained by direct calculation from the molecular-dynamics data, from the fluctuations in either the kinetic or the potential energy. The relation is

$$C=\left[1-\frac{(\Delta K)^2}{NT^2}\right]^{-1}=\left[1-\frac{(\Delta\Phi)^2}{NT^2}\right]^{-1}. \tag{5.1}$$

Here $(\Delta K)^2$ and $(\Delta\Phi)^2$ denote the mean-square fluctuation in kinetic and potential energy, respectively. Equation (5.1) is the modification appropriate for two degrees of freedom per particle[59] of a result obtained by Lebowitz, Verlet, and Percus,[60] and it is a modification appropriate to the microcanonical ensemble with conserved total energy of a familiar result for the canonical ensemble relating the specific heat to the fluctuations in the total energy.

In principle the mean-square fluctuations of kinetic and potential energy are equal, since the total energy is conserved. In molecular-dynamics calculations there are differences between these two quantities resulting from the errors generated by the numerical integration of the equations of motion. In the calculations here these two quantities deviate from their average by amounts up to 10%. Since the denominators in Eq. (5.1) become small near the transition, the values of the specific heat obtained from the two parts of Eq. (5.1) differ by amounts up to 17%.

The results for the specific heat obtained from Eq. (5.1) are shown in Fig. 6. Each point is the average of two values, and the error bars show the spread between those two values. The dashed line at the value two is the harmonic value for two degrees of

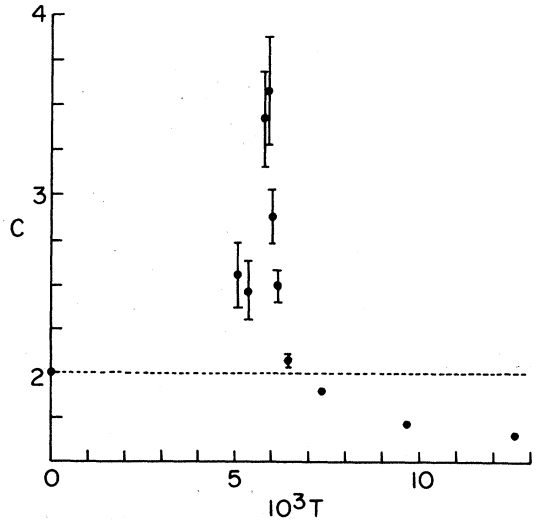

FIG. 6. Specific heat per particle vs temperature. The dots show the average of two values calculated separately from the fluctuations of kinetic and potential energy, and the error bars show the difference between those two values. The dotted line is the specific heat of a harmonic system with two degrees of freedom per particle.

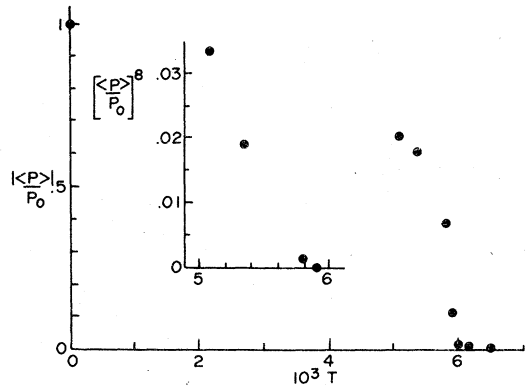

FIG. 7. Average order parameter vs temperature, and the eighth power of the average order parameter vs temperature.

freedom per particle. The large increase in the specific heat is evidence that the system undergoes a phase transition near the temperature value 6×10^{-3}.

The system orders by having the particles shift a finite amount parallel to the y axis with adjacent particles moving in opposite directions, as described in Sec. II. Thus the order parameter of the transition is the average value $\langle P\rangle$ of the fluctuating quantity

$$P(t)=N^{-1}\sum_{\vec{R}}(-1)^{l_x+l_y}u_y(\vec{R},t)\ . \tag{5.2}$$

The calculated values of $\langle P\rangle$, relative to the zero-temperature value from Eq. (2.37), as a function of temperature are shown in Fig. 7. From that figure it can be concluded that the system undergoes a continuous structural phase transition and that the transition temperature is near 6×10^{-3}, as also estimated previously from the specific heat.

The order-parameter susceptibility measures the response of the system to a time-independent external force which acts parallel to the [01] direction and pushes adjacent particles in opposite directions. This susceptibility can be calculated from the mean-square fluctuations in the order parameter, as

$$\chi_E=(N/k_BT)(\langle P^2\rangle-\langle P\rangle^2)\ . \tag{5.3}$$

The subscript denotes that the molecular-dynamics calculations give the susceptibility at constant energy rather than at constant temperature; the relation between the two quantities is[40,60]

$$\chi_E=\chi_T-\frac{k_BT}{C_v}\left(\frac{\partial\langle P\rangle_E}{\partial T}\right)^2\ . \tag{5.4}$$

Above T_c the two quantities are equal, but there is a difference in the low-temperature phase. The results for χ_E are shown in Fig. 8. There is an increase of three orders of magnitude in this quantity near the temperature 6×10^{-3}, again indicating the existence of a continuous phase transition in this system.

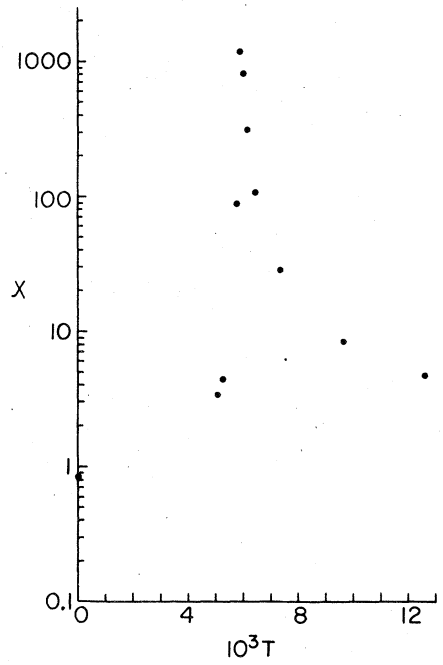

FIG. 8. Order-parameter susceptibility vs temperature.

Near the transition the temperature dependence of the order parameter and the susceptibility should be given by power laws of the form $|T-T_c|^{\pm p}$. Furthermore the universality hypothesis asserts that the values of the critical exponents are the same for all systems in the same universality class, which is determined only by the dimensionality of the system and the number of components of the order parameter. This system is two-dimensional and the order parameter has only one component, since the rectangular anisotropy described by the parameter g allows the system to order parallel to the [01] direction only, as discussed in Secs. II and III. Therefore this system is in the same universality class as the two-dimensional Ising model for which exact values of the critical exponents are known.[61] The value for the order-parameter exponent is $\beta=\frac{1}{8}$ and for the susceptibility exponent is $\gamma=\frac{7}{4}$.

The inset to the order-parameter graph in Fig. 7 shows the eighth power of $\langle P\rangle$ versus temperature, from which it is seen that there is a region of nearly linear behavior of this quantity, but that the data is too sparse and spaced over too large a temperature range to make a definite statement. A fit of power-law functions to the order-parameter data and to the susceptibility data above T_c gives the following numbers: for the transition temperature,

$$T_c=(5.90\pm0.03)\times10^{-3} \tag{5.5}$$

and for the critical exponents,

$$\beta\approx0.17\ ,\quad \gamma\approx1.18\ . \tag{5.6}$$

These values for β and γ lie between the mean-field values, $\beta_{MF}=\frac{1}{2}$ and $\gamma_{MF}=1$, and the exact values; the agreement with the exact values is not particularly good. The exact critical exponents should describe the temperature dependence in a small interval around T_c where the correlation length is much larger than both the lattice constant and the range of the forces. These results indicate that molecular-dynamics calculations with a 40×40 lattice seem not to have reached this asymptotic critical region.

As the transition is approached from the high-temperature side, the state of the system should be characterized as consisting of large regions which are ordered in one or the other of the two possible configurations of the low-temperature phase corresponding to different signs of the order parameter. The growth of these regions as the temperature decreases can be seen from the static correlation function, defined by

$$g(\vec{R})=\left[N^{-1}\sum_{\vec{R}'}(-1)^{l_x+l_y}\langle u_y(\vec{R}+\vec{R}',t)u_y(\vec{R}',t)\rangle-\langle P\rangle^2\right]/P_0^2 \ . \tag{5.7}$$

Here P_0^2 denotes the square of the zero-temperature order parameter [given in Eq. (2.37)]; this factor is included to have a convenient normalization.

If the two particles at $\vec{R}'$ and $\vec{R}'+\vec{R}$ are found in positions appropriate for either of the configurations of the low-temperature phase corresponding to different signs of the order parameter, then the contribution of that pair of particles to the sum in Eq. (5.7) is positive. Thus for temperatures somewhat above T_c and all temperatures below T_c, the sum in Eq. (5.7) is large. Subtracting the square of the average order parameter cancels most of the sum for temperatures less than T_c, so that for each $\vec{R}$, $g(\vec{R})$ becomes large only for temperatures in an interval around T_c. This increase in the range of the pair correlations is the mechanism for producing the increase in the susceptibility near T_c, since

$$\chi_E=(P_0^2/k_BT)\sum_{\vec{R}}g(\vec{R}) \ . \tag{5.8}$$

The results for $g(\vec{R})$ are shown in Fig. 9, for $\vec{R}$ parallel to [10] in the left half and to [01] in the right half, and for $T>T_c$. The increase in range of the correlations as T approaches T_c is clearly evident. At high temperature the correlations are anisotropic, extending further in the [10] direction than in the [01] direction, but this anisotropy decreases as T_c is approached. The results for $g(\vec{R})$ for $T<T_c$ look quite similar to those in Fig. 9 for $T>T_c$. At the larger $\vec{R}$ values $g(\vec{R})$ decreases quite rapidly with decreasing temperature below T_c.

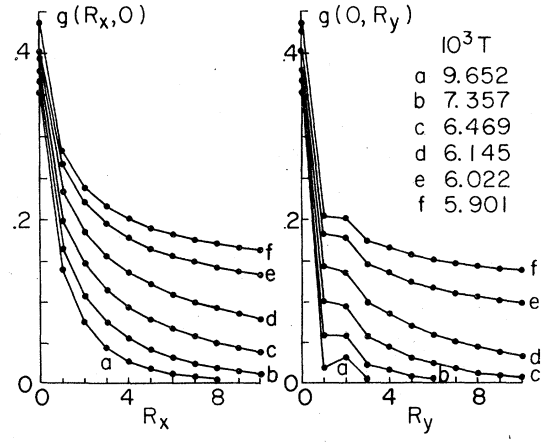

FIG. 9. Static correlation function vs distance for a sequence of temperatures above T_c. The left-hand half is for $\vec{R}$ parallel to the x axis and the right-hand half for $\vec{R}$ parallel to the y axis.

The correlations at $T=5.901\times10^{-3}$ decrease very slowly and are non-negligible if extrapolated to 40 lattice constants. This fact and anomalies in other data at this temperature, which is very close to the estimated value of T_c in Eq. (5.5), lead to the suspicion that the data at this temperature are affected by finite size effects, so the results at this temperature are omitted from the remainder of the paper.

VI. ORDER-PARAMETER CORRELATION FUNCTION

The results for the time-dependent order-parameter correlation function and its spectral function are presented in this section. This function is closely related to the scattering law measured in neutron and light scattering experiments in which the central peak has been observed.[8–14,62]

The instantaneous order parameter has been defined in Eq. (5.2). The correlation function for the fluctuations of this quantity is defined by

$$D(t)=\langle[P(t+\tau)-\langle P\rangle][P(\tau)-\langle P\rangle]\rangle \ , \tag{6.1}$$

and its spectral function by the Fourier transform relation

$$D(\omega)=\int_{-\infty}^{\infty}dt\,e^{-i\omega t}D(t) \ . \tag{6.2}$$

The quantity $\langle P\rangle$ is the average order parameter given in Sec. V. This becomes nonzero for $T<T_c$ and subtracting it off in Eq. (6.1) then becomes important.

Since the alternating sign factor $(-1)^{l_x+l_y}$ in Eq. (5.2) is the plane-wave phase factor evaluated at the soft-mode wave vector $\vec{q}_c$, as shown in Eq. (2.17),

the order parameter is proportional to the $\vec{q}_c$th spatial Fourier amplitude of the y component of the displacement field,

$$P(t) = N^{-1} \sum_{\vec{R}} e^{i\vec{q}_c \cdot \vec{R}} u_y(\vec{R}, t)$$

$$= N^{-1} u_y(\vec{q}_c, t) \ . \qquad (6.3)$$

Thus the order-parameter correlation function is also the yy tensor component of the $\vec{q}$th Fourier component of the displacement correlation function, and the spectral function $D(\omega)$ is proportional to the one-phonon approximation to the experimentally measured scattering cross section. A third interpretation of $D(t)$ as the correlation function for the $\vec{q}=0$ Fourier component of the staggered displacement field is obtained using Eq. (3.25).

The molecular-dynamics results for the time-dependent correlation functions at temperatures both above and below the transition and fairly far from it are shown in Fig. 10; the transition temperature is in the temperature interval marked by the bar in the figure. The results for temperatures in a narrow interval around T_c are in Fig. 11. The corresponding spectral functions are in Figs. 12–14. The graphs of

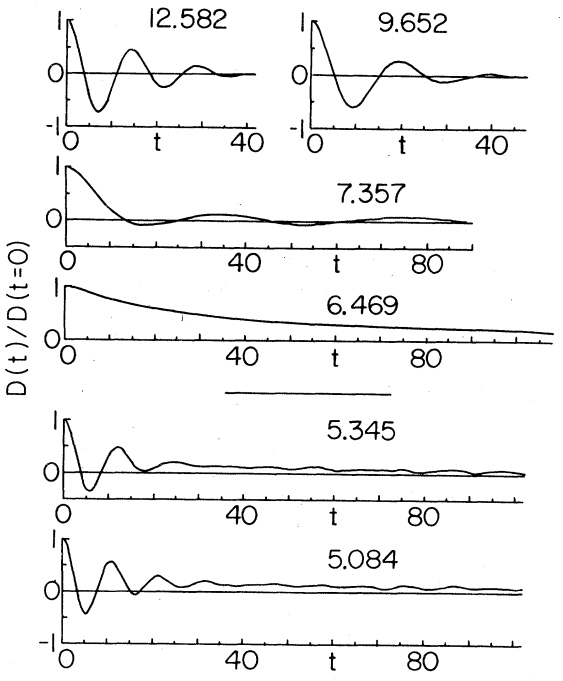

FIG. 10. Time-dependent order-parameter correlation function, normalized to the value unity at zero time. The numbers identifying each graph are 10^3T, where T is the temperature for that graph. The top four graphs are for $T > T_c$, and the bottom two graphs are for $T < T_c$.

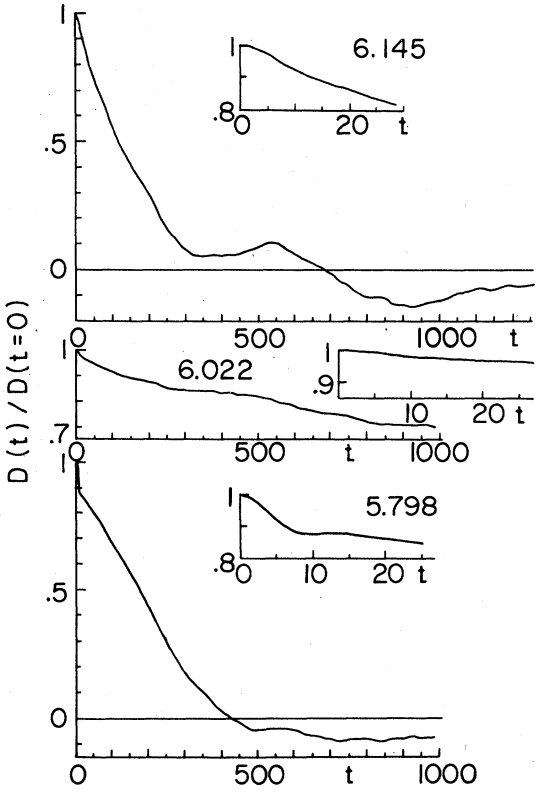

FIG. 11. Time-dependent order-parameter correlation function, normalized to the value unity at zero time. The numbers identifying each graph give the temperature as in Fig. 10. The higher-temperature graphs have $T > T_c$, and the lower-temperature graph has $T < T_c$. The time scale on the large graphs has been compressed by a factor 10 relative to Fig. 10. The small insert graphs show the short-time behavior.

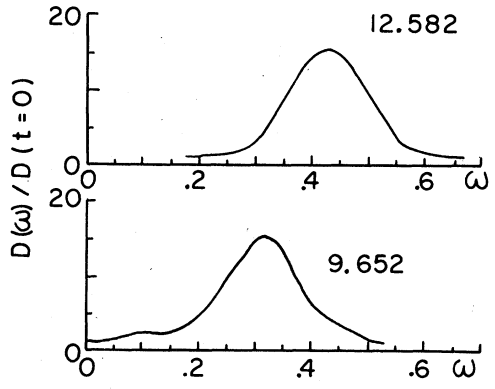

FIG. 12. Spectral functions of the order-parameter correlation function vs frequency at the two highest temperatures. The numbers identifying each graph are 10^3T where T is the temperature. The functions have been normalized by the initial value of the corresponding correlation function.

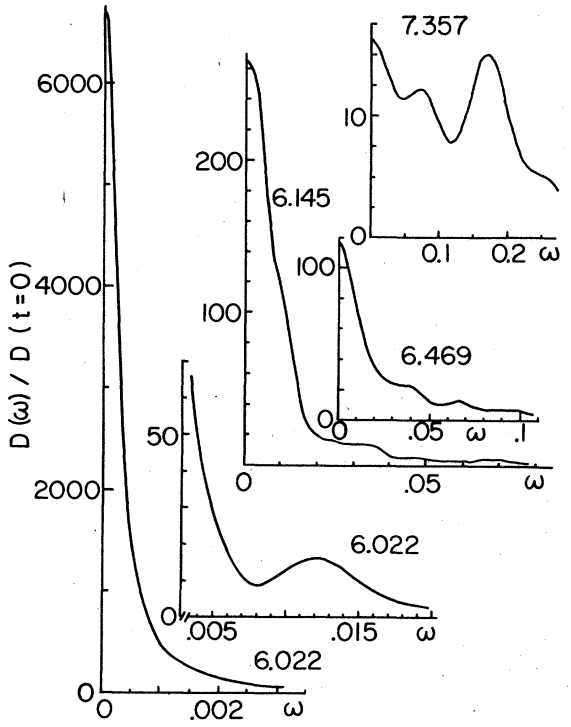

FIG. 13. Spectral functions of the order-parameter correlation function vs frequency for temperatures $T > T_c$. The numbers identifying each graph are $10^3 T$. The functions have been normalized by the initial value of the corresponding correlation function.

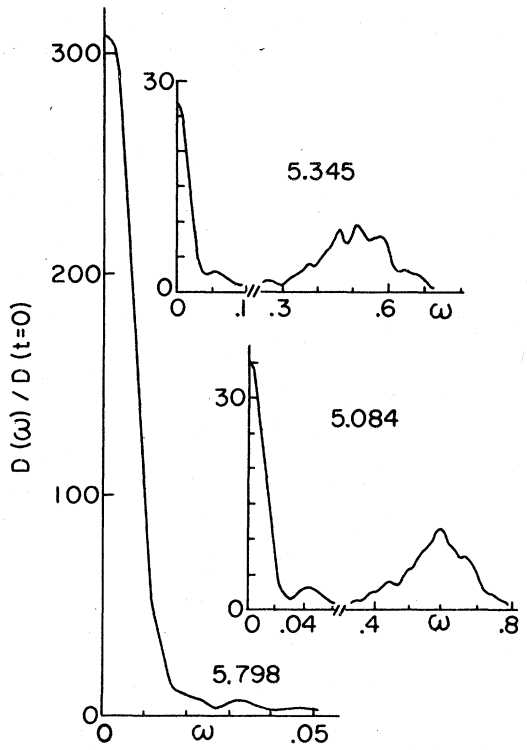

FIG. 14. Spectral functions of the order-parameter correlation function vs frequency for temperatures $T < T_c$. The numbers identifying each graph are $10^3 T$. The functions have been normalized by the initial value of the corresponding correlation function.

the correlation functions have been normalized to the value unity at $t=0$, and the spectral function graphs are the transforms of these normalized functions. The initial values $D(t=0)$ are listed in Table IV. These initial values are the mean-square fluctuations in the order parameter, hence are related to the order-parameter susceptibility as shown in Eq. (5.3) and diverge at T_c.

TABLE IV. Initial values of the order-parameter correlation function at different temperatures T.

$10^3 T$	$D(t=0)$
12.582	6.039×10^{-2}
9.652	8.156×10^{-2}
7.357	2.196×10^{-1}
6.469	7.544×10^{-1}
6.145	1.902
6.022	5.055
5.798	5.403×10^{-1}
5.345	2.334×10^{-2}
5.073	1.670×10^{-2}

At the two highest temperatures $T = 12.582 \times 10^{-3}$ and 9.652×10^{-3}, $D(t)$ has the appearance of the correlation function for an underdamped simple harmonic oscillator, with well-defined oscillations that die out after a few cycles. The spectral functions at these two temperatures are shown in Fig. 12. They show a phonon mode with well-defined frequency and lifetime, and the softening of the mode as the temperature decreases.

At $T = 7.357 \times 10^{-3}$ the oscillation frequency has decreased further, but in addition there is a change in the character of the correlation function. At the higher temperatures the areas under the positive and negative parts of the correlation function are nearly equal, as reflected in the small value of $D(\omega=0)$. However at this temperature the positive part is clearly predominant. A possible interpretation of this correlation function is as a combination of an oscillatory component and a decaying component. The spectral function at this temperature, one of the graphs in Fig. 13, shows that a central maximum has emerged. The central peak and the soft-mode peak have roughly the same intensities and widths at this temperature.

There is an additional maximum near $\omega=0.1$ on this spectral function. Its existence has been checked by varying the time and manner of the cutoff on the correlation function, and it persists throughout these modifications. It is believed to be a real effect caused by some subtlety in the way that $D(t)$ decays to zero. Similar peaks additional to the central peak and soft-mode peak have been found by Aubry in calculations for a one-dimensional system.[21]

At $T=6.469\times10^{-3}$ the correlation function has essentially completely ceased oscillating and has become a very slowly relaxing function. It passes through zero at $t=516$, beyond the scale of the graph. For the (normalized) spectral function shown in Fig. 13 the central peak has increased by a factor of about 8 over its value at the previous temperature. The soft-mode peak is near $\omega=0.07$ with an intensity that is small relative to the central peak but which has about the same intensity as at the previous temperature. In addition there is a broad shoulder on $D(\omega)$ in the region $\omega=0.03-0.04$ whose origin may be related to the additional maximum near $\omega=0.1$ that was observed at the previous temperature.

The time correlation functions at temperatures fairly far from the transition shown in Fig. 10 decay on a time scale extending approximately to $t=100$. For temperatures closer to the transition, the time variation occurs on a much longer time scale, so the correlation functions for these temperatures are shown in Fig. 11, where the time axis is extended out to $t=1000$. The short time behavior is shown by the inserts at each temperature.

At $T=6.145\times10^{-3}$ the time variation of the order parameter has become very slow, and the correlation function gets through only two oscillations over this extended time interval. The intensity of the central peak in the spectral function (Fig. 13) has increased again. The soft-mode frequency is near $\omega=0.035$, and there is a hint of a shoulder on the side of the central peak near $\omega=0.01$.

The correlation function at $T=6.022\times10^{-3}$, which is the lowest temperature above T_c for which calculations were done, is the center graph in Fig. 11. Over the time interval from $t=0$ to $t=1000$, $D(t)$ decays only by about 30% from its initial value. At this temperature, the order parameter has become practically a stationary quantity.

The spectral function at $T=6.022\times10^{-3}$ is shown in the two graphs on the left-hand side of Fig. 13. These two curves are continuations of each other; the smaller one has an expanded vertical scale and compressed horizontal scale to bring out the soft-mode peak at $\omega=0.0119$. This soft-mode peak results from the very small and slow oscillations which are barely visible in Fig. 11 superimposed on the even slower decay of the correlation function.

The central peak at $T=6.022\times10^{-3}$ is very strong and very narrow. Its intensity is about 450 times that of the soft-mode peak, and its width is about one-tenth the width of the soft-mode peak at the same temperature. Furthermore the ratio of the width of the central peak at this temperature to the width of the soft phonon peak at $T=9.652\times10^{-3}$ where there is no central peak is about 4×10^{-3}. This very large magnitude of the central peak is the major feature by which the results of these molecular-dynamics calculations differ from the results obtained by Schneider and Stoll,[40] who find central peaks which are of the order of 20 times the soft-mode peaks obtained at the same temperature. The spectral functions illustrated in these figures have been normalized by the initial value of the correlation function $D(t=0)$. Experimental spectra are not usually normalized that way, and for experimental comparison it is more useful to use the un-normalized value at zero frequency. Over the temperature range shown in Fig. 13, $D(\omega=0)$ increases by a factor of 8000. The magnitude of the growth of the central peak found here is quite comparable to the experimental results obtained for $SrTiO_3$,[9] and it increases confidence in the viewpoint that the experimentally observed central peaks can be explained as the result of anharmonic mechanisms intrinsic to the pure crystal and that it is not necessary to invoke impurity mechanisms.[30,31]

The correlation function at the bottom of Fig. 11 is for temperature $T=5.798\times10^{-3}$ which is in the ordered phase. The order parameter has now obtained a nonzero value, and this is the correlation function for the fluctuations about that value. The rate of variation has now increased so that this correlation function appears similar to the one at $T=6.145\times10^{-3}$ above T_c. The short-time behavior of this function is rather interesting. As shown by the small insert in Fig. 11 over the interval from $t=0$ to $t=10$ the correlation function decays rapidly through about 10% of its initial value, and then a slower decay takes over. Correlation functions with this type of initial behavior will be seen again in Sec. VII where the dependence on wave vector will be studied. The spectral function for this temperature is shown in Fig. 14. The central-peak intensity has decreased considerably, and the soft-mode peak has moved out to higher frequency.

The correlation functions for order-parameter fluctuations at lower temperatures are shown back in Fig. 10 at the bottom of the figure. These correlation functions again have the appearance of damped simple harmonic oscillator functions, as at the highest temperatures discussed above, except that they have a part which decays very slowly at long times. It is possible that this tail is due to numerical errors in the calculation of the correlation function. Since $T<T_c$ here, the square of the nonzero order parameter must be subtracted from the calculation of the correlations in order to obtain the correlation function for the fluctuations. If an incorrect value were subtract-

ed, then the correlation function will approach some nonzero value for long times. An argument that this has been done properly is that these correlation functions do pass through zero, although at times that are beyond the scale of the graph in Fig. 10. At $T=5.345\times10^{-3}$ the correlation function passes through zero at $t=142$, and at $T=5.084\times10^{-3}$ it passes through zero at $t=328$. In addition, care was taken in calculating these correlation functions, namely, they were calculated as $\langle P(t+\tau)[P(\tau)-\langle P\rangle]\rangle$, the averaging interval on τ was kept the same for all t values, and that same interval was used to calculate $\langle P\rangle$. For these reasons it is felt that the long tails on $D(t)$ at the lowest temperatures are a real effect, even though taking differences of large numbers is involved in calculating $D(t)$ for $T<T_c$.

The spectral functions for these two lowest temperatures are shown in Fig. 14. They have central peaks due to the slow decay of the correlation functions. The soft-mode frequency increases as the temperature decreases, and the soft-mode peak has a substantial fraction of the total spectral weight. The central-peak height at the lowest temperature $T=5.084\times10^{-3}$ is slightly higher than at the higher temperature $T=5.345\times10^{-3}$, i.e., it appears that as the temperature decreases below T_c the central-peak height first decreases and then starts to increase again. The mathematical reason for this is that the slowly decaying tail on these correlation functions lasts longer at the lowest temperature, as is evident from the numbers given in the preceding paragraph. With only one data point showing this effect it is difficult to be certain that it is real, but it is consistent with the experimental results on lead germanate obtained by Axe, Cowley, and Iizumi,[13] who found that the central-peak intensity decreased below the transition and then increased again.

The correlation functions at the two lowest temperatures can be understood to have evolved continuously from that at $T=5.798\times10^{-3}$ if the correlation functions are considered to be superpositions of a rapidly varying contribution and a slowly varying contribution. At $T=5.798\times10^{-3}$ the rapidly varying part causes the initial rapid decay, but it has small amplitude and damps quickly at this temperature so that after $t=10$ the slowly varying component is all that remains. At the lowest temperatures the relative magnitudes of the two components are interchanged. The rapidly varying component has become oscillatory, and it dies out near $t=30$, leaving the slowly varying component which has a much reduced amplitude at these lower temperatures.

The square of the soft-mode frequency as obtained from all of the previous graphs for the spectral functions is plotted versus temperature in Fig. 15. Excluding the points near T_c, $\omega^2(\vec{q}_c)$ can be closely fit by linear functions of temperature above and below T_c,

$$\omega^2(\vec{q}_c)=\begin{cases}28.55|T-6.278\times10^{-3}|\,, & T>T_c\ ,\\ 277.3|T-6.278\times10^{-3}|\,, & T<T_c\ .\end{cases} \tag{6.4}$$

The intercept of these lines on the temperature axis is at a slightly higher temperature than was estimated for the critical temperature from the static properties in Eq. (5.5). A linear dependence on temperature is predicted by mean-field theory.[3] Near T_c, $\omega^2(\vec{q}_c)$ deviates from this linear behavior and seems to remain nonzero at T_c; this is not obvious from Fig. 15, but from Fig. 13 it is clear that $\omega^2(\vec{q}_c)$ is nonzero at

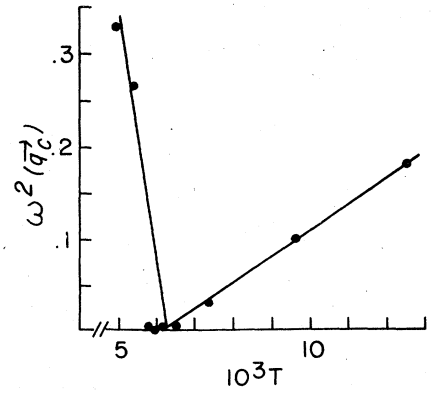

FIG. 15. Square of the soft-mode frequency vs temperature. The straight lines are fits to the points away from the immediate neighborhood of T_c.

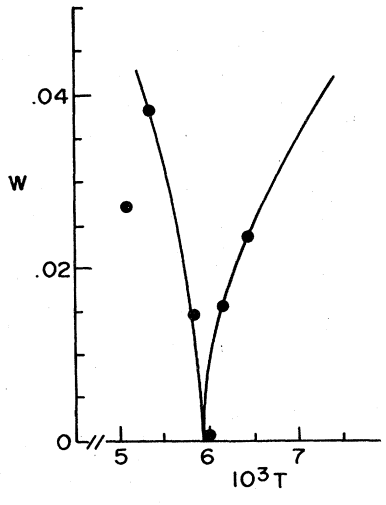

FIG. 16. Full width at half maximum of the central peak vs the temperature. The solid curve is the fit of the power-law formula in Eq. (6.5) to the data, using $T_c=5.90\times10^{-3}$.

$T=6.022\times10^{-3}$. This overall behavior of the soft-mode frequency is precisely the same as is observed for $SrTiO_3$.[9]

A plot of the full width at half maximum of the central peak $W(T)$ versus temperature is given in Fig. 16. The solid lines are fits of a power law $A|T-T_c|^p$ to all the data *except* the point at $T=6.022\times10^{-3}$ and the lowest temperature at $T=5.084\times10^{-3}$, using the value for T_c determined in Eq. (5.5). Constraining the exponent to have the same value above and below T_c, the best fit is given by the functions

$$W(T)=\begin{cases}0.08835\left(\dfrac{T}{5.90\times10^{-3}}-1\right)^{0.55}, & T>T_c\ ,\\[2ex] 0.1392\left(1-\dfrac{T}{5.90\times10^{-3}}\right)^{0.55}, & T<T_c\ ,\end{cases} \tag{6.5}$$

i.e., with the value of the exponent close to $\frac{1}{2}$. Thus one can say that in the temperature interval where $\omega^2(\vec{q}_c)$ has a linear dependence on temperature, the central-peak width has essentially a square-root dependence. The central-peak width at $T=6.022\times10^{-3}$ is excluded from this fit because it is clearly considerably narrower than is given by the function in Eq. (6.5), and a crossover between two different temperature dependences may occur very near the transition. The point at $T=5.084\times10^{-3}$ is excluded because the width decreases at that temperature in conjunction with the increase in the magnitude of the central peak which was noted in the previous discussion in this section; this low-temperature phenomenon should be excluded from a power-law fit designed for use near the transition. It seems reasonable to conclude from these calculations that the central-peak width has a power-law dependence on temperature near T_c, but in view of the lack of agreement of the static critical exponents obtained in Sec. V with the theoretical values and the paucity of data here, any numerical values determined for the exponents must be taken *cum grano salis*.

The results for the order-parameter correlation function presented in this section are in substantial agreement with the experiments with respect to the temperature dependence of the soft-mode frequency and the very large intensity and very narrow width of the central peak. This agreement is in favor of the view that the anharmonic forces of the model used for the calculations have captured the essential features of the phenomena observed at structural phase transitions.

VII. WAVE-VECTOR-DEPENDENT CORRELATION FUNCTIONS

The time-dependent order-parameter correlation function $D(t)$ was written in several different forms in Sec. VI: as the correlation function either for displacement fluctuations at $\vec{q}=\vec{q}_c$ or for the staggered displacement fluctuations at $\vec{q}=0$. In this section those calculations are extended to correlation functions for displacement fluctuation patterns which differ from the soft-mode pattern, i.e., for other values of the wave vector.

The doubling of the unit cell of the lattice and the resulting change in the Brillouin zone of the lattice at T_c introduces a complication into the calculation; the wave vector region of interest is around $\vec{q}_c$ which is a zone corner for $T>T_c$ and a zone center for $T<T_c$. This change is shown in Fig. 2 and in the related discussion in Sec. II. It is desirable, both for obtaining the correlation functions from the molecular-dynamics data and for displaying the results, to use a unified description which applies to both the high- and low-temperature phases. The way to do this has been given by Nelson and Fisher[63] and by Kosterlitz, Nelson, and Fisher.[64]

The lattice points are partitioned into two interpenetrating sublattices, A and B, according to the value of the phase factor

$$e^{-i\vec{q}_c\cdot\vec{R}}=\begin{cases}+1, & \vec{R}\in A\\ -1, & \vec{R}\in B\end{cases} \tag{7.1}$$

and the displacements on these two sublattices are considered to be two separate functions $\vec{u}^{(A)}(\vec{R},t)$ and $\vec{u}^{(B)}(\vec{R},t)$, respectively. It is necessary to introduce these two functions to describe the low-temperature phase, and it is acceptable to use them for describing the high-temperature phase.

The spatial Fourier transforms of these two functions are defined by

$$\vec{u}^{(A)}(\vec{q},t)=\sum_{\vec{R}\in A}e^{-i\vec{q}\cdot\vec{R}}\vec{u}(R,t)\ ,\qquad \vec{q}\in Z_{\mathrm{LT}} \tag{7.2}$$

and by a similar equation for the B sublattice. The wave vectors in Eq. (7.2) are restricted to the Brillouin zone of the low-temperature phase, which is the inner square in Fig. 2 and is denoted by Z_{LT} in Eq. (7.2). The correlation functions are now most usefully described in terms of the functions

$$\vec{u}^{(\pm)}(\vec{q},t)=\tfrac{1}{2}[\vec{u}^{(A)}(\vec{q},t)\pm\vec{u}^{(B)}(\vec{q},t)]\ . \tag{7.3}$$

The function $\vec{u}^{(+)}(\vec{q},t)$ is related to the lattice displacements by

$$\vec{u}^{(+)}(\vec{q},t)=\tfrac{1}{2}\sum_{\vec{R}}e^{-i\vec{q}\cdot\vec{R}}\vec{u}(\vec{R},t)\ ,\qquad \vec{q}\in Z_{\mathrm{LT}}\ , \tag{7.4}$$

with the sum being over all of the lattice sites. In the high-temperature phase where all the lattice sites are equivalent, $\vec{u}^{(+)}(\vec{q}, t)$ is proportional to the spatial Fourier amplitudes of the displacement field, but only for $\vec{q} \in Z_{LT}$. Similarly, by using Eq. (7.1), $\vec{u}^{(-)}(\vec{q}, t)$ is related to the lattice displacements by

$$\vec{u}^{(-)}(\vec{q}, t) = \frac{1}{2} \sum_{\vec{R}} e^{-i\vec{q}\cdot\vec{R}} e^{-i\vec{q}_c\cdot\vec{R}} \vec{u}(\vec{R}, t) , \quad \vec{q} \in Z_{LT} , \tag{7.5}$$

with the sum again being over all of the lattice sites. In the high-temperature phase, $\vec{u}^{(-)}(\vec{q}, t)$ can be thought of either as being proportional to $\vec{u}(\vec{q}_c + \vec{q}, t)$, the Fourier amplitudes of the displacement field in the portions of the high-temperature Brillouin zone which are *not* in the low-temperature Brillouin zone, or as being proportional to $\vec{S}(\vec{q}, t)$, the Fourier amplitudes of the staggered displacement field, but only for $\vec{q} \in Z_{LT}$. Furthermore, for all temperatures, as $\vec{q}$ approaches zero $u_y^{(-)}(\vec{q}, t)$ be-

TABLE V. Initial values of the displacement correlation function at different temperatures T and wave vectors $\vec{q}$. The wave vector $\vec{q}^*$ with integer components identifies $\vec{q}$ in the manner described in the text in Sec. VII.

$10^3 T$	$\vec{q}^*$	$D(\vec{q}, t=0)$	$10^3 T$	$\vec{q}^*$	$D(\vec{q}, t=0)$
7.357	(0,2)	7.525×10^{-2}		(1,1)	7.524×10^{-2}
	(0,4)	3.404×10^{-2}		(2,2)	2.254×10^{-2}
	(2,0)	3.038×10^{-2}		(3,3)	1.221×10^{-2}
	(4,0)	1.078×10^{-2}		(4,4)	7.392×10^{-3}
	(2,2)	2.986×10^{-2}	5.798	(0,1)	2.002×10^{-1}
	(4,4)	9.658×10^{-3}		(0,2)	5.658×10^{-2}
6.469	(0,2)	1.152×10^{-1}		(0,3)	3.433×10^{-2}
	(0,6)	1.970×10^{-2}		(0,4)	2.351×10^{-2}
	(2,0)	3.252×10^{-2}		(0,6)	1.359×10^{-2}
	(4,0)	9.071×10^{-3}		(1,0)	5.228×10^{-2}
	(2,2)	2.806×10^{-2}		(2,0)	2.077×10^{-2}
	(4,4)	8.615×10^{-3}		(3,0)	1.088×10^{-2}
6.145	(0,1)	4.161×10^{-1}		(4,0)	6.615×10^{-3}
	(0,2)	1.325×10^{-1}		(1,1)	4.832×10^{-2}
	(0,3)	6.317×10^{-2}		(2,2)	1.841×10^{-2}
	(0,4)	3.778×10^{-2}		(3,3)	9.721×10^{-3}
	(0,6)	1.801×10^{-2}		(4,4)	6.594×10^{-3}
	(1,0)	1.151×10^{-1}	5.345	(0,1)	1.722×10^{-2}
	(2,0)	3.262×10^{-2}		(0,2)	1.403×10^{-2}
	(3,0)	1.529×10^{-2}		(0,3)	1.308×10^{-2}
	(4,0)	8.617×10^{-3}		(0,4)	1.144×10^{-2}
	(1,1)	1.008×10^{-1}		(1,0)	1.494×10^{-2}
	(2,2)	2.768×10^{-2}		(2,0)	1.062×10^{-2}
	(3,3)	1.308×10^{-2}		(3,0)	7.095×10^{-3}
	(4,4)	8.229×10^{-3}		(4,0)	5.236×10^{-3}
6.022	(0,1)	2.957×10^{-1}		(1,1)	1.429×10^{-2}
	(0,2)	1.057×10^{-1}		(2,2)	9.571×10^{-3}
	(0,3)	5.433×10^{-2}		(3,3)	6.709×10^{-3}
	(0,4)	3.274×10^{-2}		(4,4)	4.677×10^{-3}
	(0,6)	1.619×10^{-2}			
	(1,0)	9.569×10^{-2}			
	(2,0)	2.755×10^{-2}			
	(3,0)	1.375×10^{-2}			
	(4,0)	7.778×10^{-3}			

comes proportional to the instantaneous order parameter $P(t)$ defined in Eq. (5.2). Therefore it is the correlation function and spectral function of $u_y^{(-)}(\vec{q}, t)$ for $\vec{q}$ around zero which should be computed to investigate how the features of the order-parameter correlation function depend on wave vector, both above and below T_c.

Consequently, the correlation function

$$D(\vec{q}, t) = (N/2)^{-1}\langle u_y^{(-)}(\vec{q}, t) u_y^{(-)}(-\vec{q}, 0)\rangle \tag{7.6}$$

and the corresponding spectral function

$$D(\vec{q}, \omega) = \int_{-\infty}^{\infty} dt\, e^{-i\omega t} D(\vec{q}, t)\ , \tag{7.7}$$

have been computed as a function of temperature and wave vector from the molecular-dynamics data. This correlation function is related to the order-parameter correlation function defined in Eq. (6.1) by

$$D(\vec{q}=0, t) = (N/2) D(t)\ . \tag{7.8}$$

The results obtained for these functions are shown in Figs. 17 through 27. These calculations were done

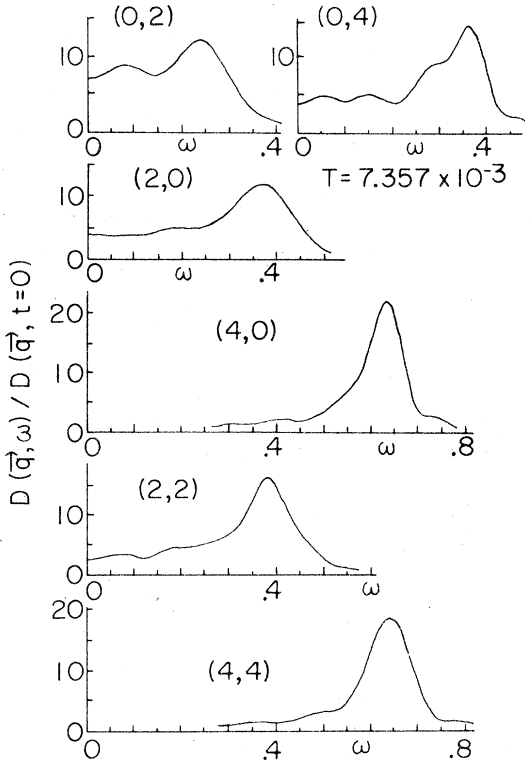

FIG. 17. Spectral functions vs frequency for the wave-vector-dependent displacement correlation function at temperature $T = 7.357\times10^{-3}$. The integer pair with each graph identifies the wave vector $\vec{q}$ according to the prescription for periodic boundary conditions as described in the text. Each graph is normalized by the initial value of the corresponding correlation function.

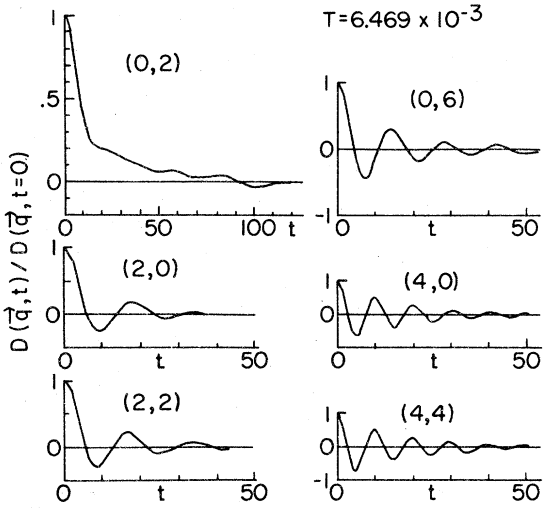

FIG. 18. Time-dependent and wave-vector-dependent correlation function at temperature $T = 6.469\times10^{-3}$. The integer pair with each graph identifies the wave vector as described for Fig. 17. Each function is normalized to the value unity at zero time.

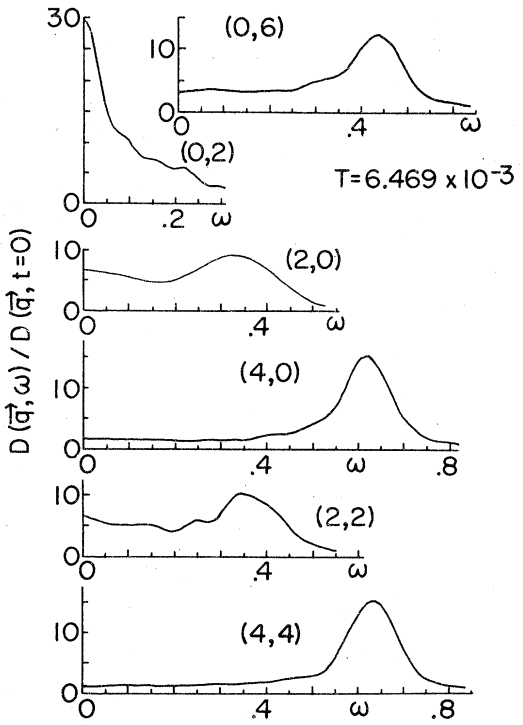

FIG. 19. Spectral functions vs frequency for the normalized wave-vector-dependent displacement correlation functions shown in Fig. 18. The integer pair with each function identifies the wave vector for that function as described for Fig. 17.

for all the temperatures for which the molecular-dynamics calculations were done, and most of the results for the spectral functions are shown here. In addition, for $T \leq 6.469\times10^{-3}$ the time-dependent correlation functions are presented, because the behavior of these functions changes considerably with wave vector and it is not always clear what the time dependence is from seeing the frequency dependence of the Fourier transform. In all cases the time correlation functions have been normalized to the value unity at $t=0$, and the spectral functions shown are the Fourier transforms of these normalized functions. The initial values of the correlation functions are given in Table V. At each temperature functions for several wave vectors parallel to the [01], [10], and [11] directions are shown. The periodic boundary conditions used in the calculation require that the wave vectors have the form $\vec{q}=(2\pi/N_s a)(m_x,m_y)$, where m_x and m_y are integers and $N_s=40$ in these calculations. The integer pair (m_x,m_y) is denoted by $\vec{q}^{\,*}$ and used to identify the graphs in the figures and the text.

The spectral functions at $T=9.652\times10^{-3}$ have been calculated but are not shown here because they have typical anharmonic phonon line shapes similar to that shown for the order parameter spectral function at the same temperature in Fig. 12. The phonon frequency is found to increase slightly as $\vec{q}$ changes away from zero.

The spectral functions for $T=7.357\times10^{-3}$ are in Fig. 17. This is the highest temperature for which a central peak is obtained in the order-parameter correlation function, shown in Fig. 13. At nonzero wave vector there is still spectral weight at zero frequency at $\vec{q}^{\,*}=(0,2)$, (0,4), and (2,0), and then the line shapes revert to well-defined phonon peaks at larger wave vectors. Anisotropy is evident from these graphs in that the zero-frequency spectral weight decreases more slowly for the wave vectors parallel to [01] than for those parallel to [10]. This anisotropy persists at lower temperatures and recalls the anisotropy observed in the static correlation function $g(\vec{R})$ shown in Fig. 9. Presumably the rectangular symmetry of the potential-energy function is responsible for this anisotropic behavior. The final point to note is the additional maximum near $\omega=0.07$ for $\vec{q}^{\,*}=(0,2)$; this is related to the additional maximum in the order-parameter correlation function at this temperature (see Fig. 13).

The time-dependent correlation functions and spectral functions at $T=6.469\times10^{-3}$ are in Figs. 18 and 19, respectively. The behavior of the correlation function at $\vec{q}^{\,*}=(0,2)$ near $t=15$ shows a feature

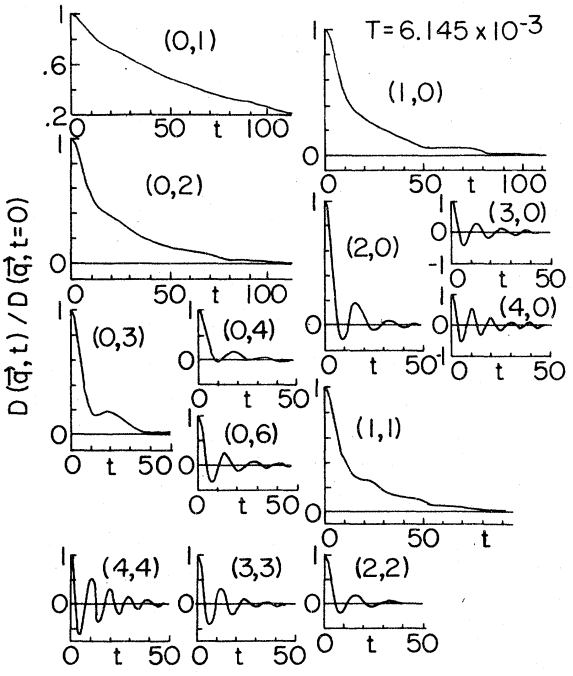

FIG. 20. Time-dependent and wave-vector-dependent correlation function at temperature $T=6.145\times10^{-3}$. The integer pair with each graph identifies the wave vector as described for Fig. 17. Each function is normalized to the value unity at zero time.

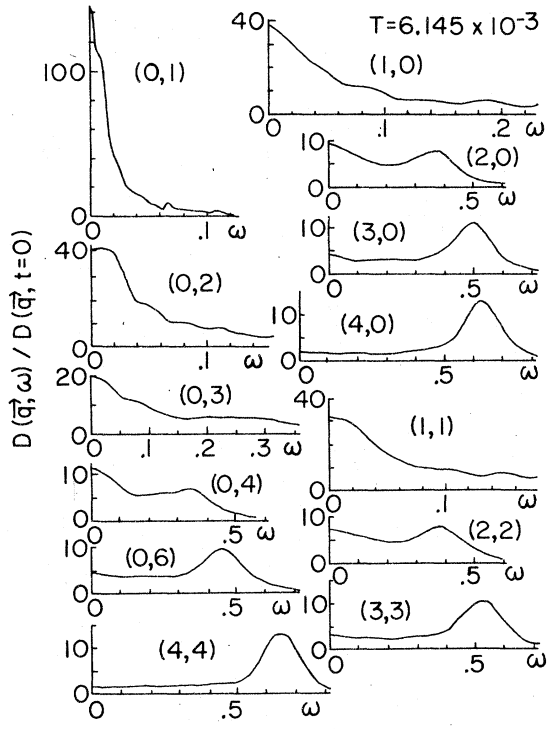

FIG. 21. Spectral functions vs frequency for the normalized wave-vector-dependent displacement correlation functions shown in Fig. 20. The integer pair with each function identifies the wave vector for that function as described for Fig. 17.

which becomes more extensive in wave vector space at lower temperatures. Namely, this particular correlation function initially decreases rapidly up to about $t=15$, and after that it is dominated by a slow decay going on to about $t=100$. The same behavior was noted in Sec. VI for the order-parameter correlation functions. This is further corroboration of the existence of processes in the dynamics of the system which occur on two different time scales. The slow decay of course manifests itself in the spectral function for this $\vec{q}$ value by the dominating central peak. The same inference concerning the existence of processes with two different time scales but with a much reduced strength of the slow process can be made from the spectral functions at $\vec{q}^{\,*}=(2,0)$ and (2,2) because these functions have small maxima at zero frequency in addition to the phonon peaks. Continuing on out to larger wave vectors, the zero-frequency spectral weight decreases to nearly vanishing intensity and the spectral functions revert to the normal anharmonic line shapes. The anisotropy noted previously is again evident in the persistence of greater zero-frequency spectral weight out to larger wave vectors parallel to [01] than for other directions.

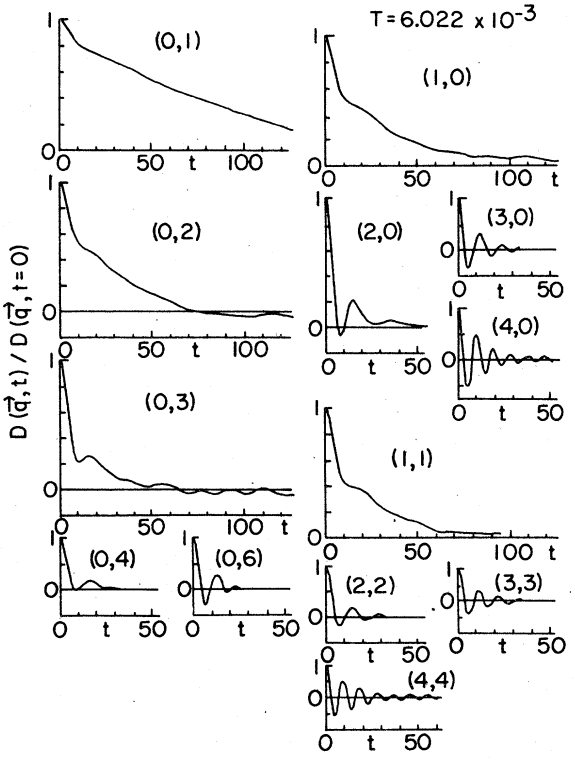

FIG. 22. Time-dependent and wave-vector-dependent correlation function at temperature $T=6.022\times10^{-3}$. The integer pair with each graph identifies the wave vector as described for Fig. 17. Each function is normalized to the value unity at zero time.

Figures 20 and 21 show the correlation functions and spectral functions for $T=6.145\times10^{-3}$. Considerably more wave vectors were studied at this and lower temperatures than at the higher temperatures. The correlation function at $\vec{q}^{\,*}=(0,1)$ consists almost entirely of a slowly decaying component, although there is a small initial interval extending out to about $t=10$ over which the decay appears to be more rapid. The rapid initial decay and then the onset of the slow decay is more clearly seen in the correlation functions at

$$\vec{q}^{\,*}=(0,2),\ (0,3),\ (0,4),\ (1,0),\ (2,0),\ (1,1)\ .$$

Looking at the spectral functions, a new effect first appears very weakly at this temperature. Namely, at the wave vector $\vec{q}^{\,*}=(0,2)$ the central peak shifts slightly or splits so that the maximum is at a small finite frequency rather than at precisely zero frequency. This splitting becomes more pronounced at lower temperatures and extends to a larger region in wave vector space. Schneider and Stoll have also found such a splitting in their calculations.[39,40]

The correlation functions and spectral functions at $T=6.022\times10^{-3}$ are in Figs. 22 and 23, respectively. This is the temperature at which the central peak in the order-parameter correlation function is most intense. Comparison of the sets of spectral functions

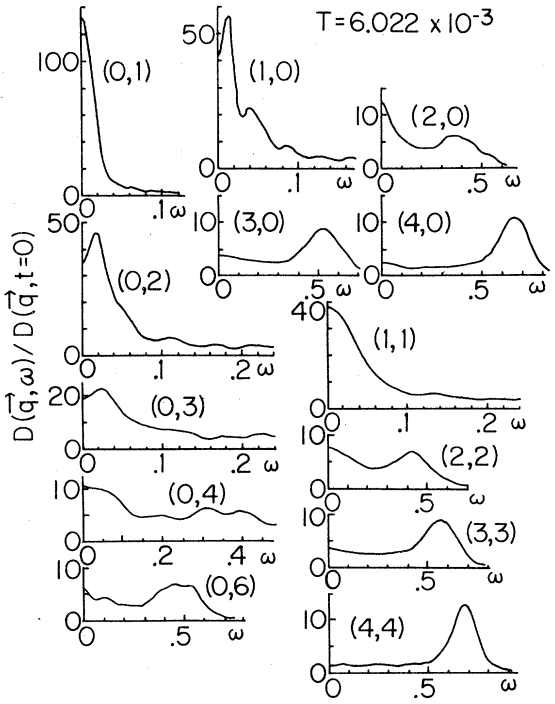

FIG. 23. Spectral functions vs frequency for the normalized wave-vector-dependent displacement correlation functions shown in Fig. 22. The integer pair with each function identifies the wave vector as described for Fig. 17.

for different temperatures shows that the central peak extends over the largest region in wave vector space at this temperature. The existence of two time scales is again evident in the correlation functions at

$$\vec{q}^{\,*} = (0,1),\ (0,2),\ (0,3),\ (0,4),$$
$$(1,0),\ (2,0),\ (1,1),\ (2,2)\ .$$

At $\vec{q}^{\,*} = (0,1)$ the initial rapid decay is very small and lasts only out to about $t = 10$. As $\vec{q}$ increases, the initial rapid decay becomes more pronounced, and when $\vec{q}$ reaches (0,3), (2,0), or (2,2), the initial decay has become a fairly long lived oscillation superimposed on a slowly decaying component. Turning to the spectral functions in Fig. 23, the most notable new feature is the increase in the size of the wave vector region in which the central peak splits, which now occurs at $\vec{q}^{\,*} = (0,2)$, (0,3), and (1,0). The magnitude of the splitting here is much more pronounced than in the spectral functions for the previous temperature. The region in wave-vector space where this split central peak occurs is a small region around but not including $\vec{q} = 0$. As $\vec{q}$ moves further out from zero, the maximum returns to zero frequency, as seen at $\vec{q}^{\,*} = (0,4)$ and (2,0), and then for even larger wave vectors, the central peak completely disappears. Thus the region with the split central peak is contained within the region of wave-vector space where the central peak appears.

Up to this point the results presented have been for temperatures above T_c. The main results are that the central peak exists in an anisotropic region around the soft-mode wave vector. This region expands as T comes closer to T_c. Within this region and within a small temperature interval above T_c, there is another smaller wave-vector region in which the central peak splits to a small finite frequency; this region also grows as T approaches T_c. As $\vec{q}$ moves further out, the spectral functions make a smooth transition to more normal anharmonic line shapes.

When T goes below T_c, similar changes occur but in reverse order. The central peak weakens in intensity, although it never completely disappears at all the temperatures at which the calculations were done. The region with the split central peak shrinks rapidly and disappears not too far below T_c.

The results for $T = 5.798\times10^{-3}$ are shown in Figs. 24 and 25. Looking at the correlation functions, the existence of two time scales is clearly evident here even at the smallest wave vectors. At $\vec{q}^{\,*} = (0,1)$, there is a definite break in the correlation function at about $t = 15$; at the higher temperatures presented

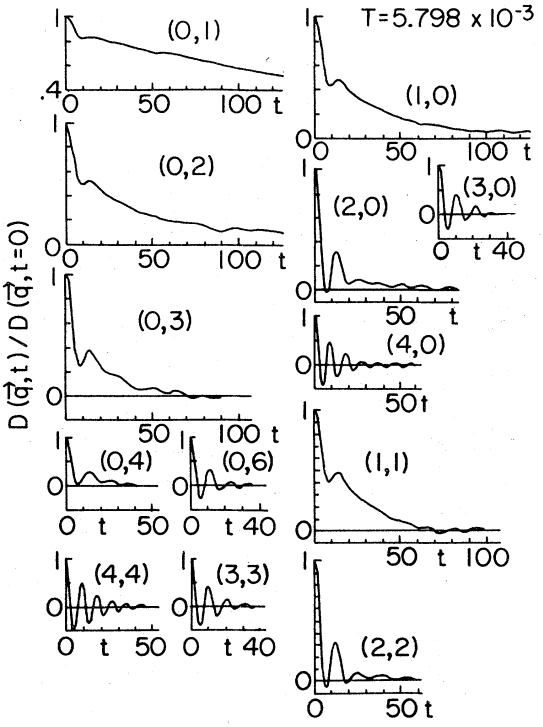

FIG. 24. Time-dependent and wave-vector-dependent correlation function at temperature $T = 5.798\times10^{-3}$. The integer pair with each graph identifies the wave vector as described for Fig. 17. Each function is normalized to the value unity at zero time.

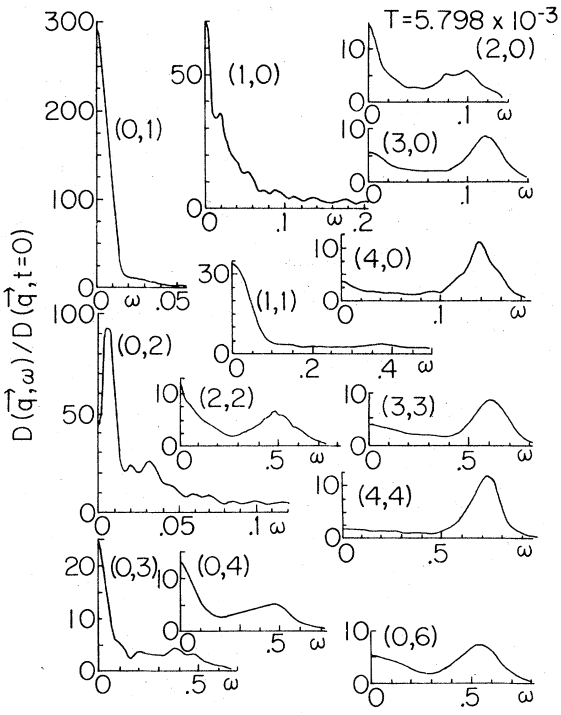

FIG. 25. Spectral functions vs frequency for the normalized wave-vector-dependent displacement correlation functions shown in Fig. 24. The integer pair with each function identifies the wave vector for that function as described for Fig. 17.

previously this break was not so clearly present at this small wave vector. Concerning the split central peaks it occurs now only at $\vec{q}^{\,*} = (0, 2)$.

The results for $T = 5.345 \times 10^{-3}$ are shown in Figs. 26 and 27. The existence of two time scales is clearly seen at practically all wave vectors here, and especially at the smallest wave vectors. At $\vec{q}^{\,*} = (0, 1)$, the correlation function is definitely oscillatory and goes through at least five complete oscillations before they damp out. Yet these oscillations are superimposed on a slowly decaying component of sufficient strength that the correlation function remains positive throughout the oscillations. The same behavior also occurs at $\vec{q}^{\,*} = (1, 0)$ and (1,1). As $\vec{q}$ increases in magnitude, the changes in the correlation function are characterized by the decrease in strength of the slowly varying component, leaving only the oscillatory component. Both components are clearly evident at all but the largest wave vectors, such as $\vec{q}^{\,*} = (4, 0)$ and (4,4). The same characterization holds also for the spectral functions. At all but the largest wave vectors there are clearly distinct central-peak and phonon contributions. At the smallest $\vec{q}$ vectors this is in contrast to the behavior at higher temperatures where there was a strong central peak, but no clearly defined phonon peak. Finally, at this temperature there is no split central peak at any wave vector.

At $T = 5.345 \times 10^{-3}$ comparison of the spectral function at $\vec{q}^{\,*} = (0, 1)$ with the order-parameter spectral function in Fig. 14 shows that the central peak is more intense at $\vec{q}^{\,*} = (0, 1)$ than at (0,0). This might be due to the possible numerical errors in the calculation of the order-parameter correlation function discussed near the end of Sec. VI, namely, that taking the difference of large numbers is involved in calculating $D(t)$ for $T < T_c$. No such problem enters in calculating $D(\vec{q}, t)$ for nonzero $\vec{q}$.

The correlation functions and spectral functions at $T = 5.084 \times 10^{-3}$ have been calculated. They are very similar to those just shown for $T = 5.345 \times 10^{-3}$, so the figures are not included here.

Most of the quantities mentioned in this section, such as the central-peak intensity, increase as T approaches T_c from above and then decrease as T goes below T_c. Therefore it is of interest to observe that at least one quantity changes in a monotonic way through the transition. This quantity is the relative strength of the rapidly varying component of the correlation function compared to the slowly decaying part. It can be observed in the temperature dependence of the correlation function at the single wave vector $\vec{q}^{\,*} = (0, 1)$; the same behavior is also evident at the neighboring wave vectors. At $T = 6.145 \times 10^{-3}$ there is a very slight break in this curve near $t = 15$ as the function changes from a slightly faster decay to

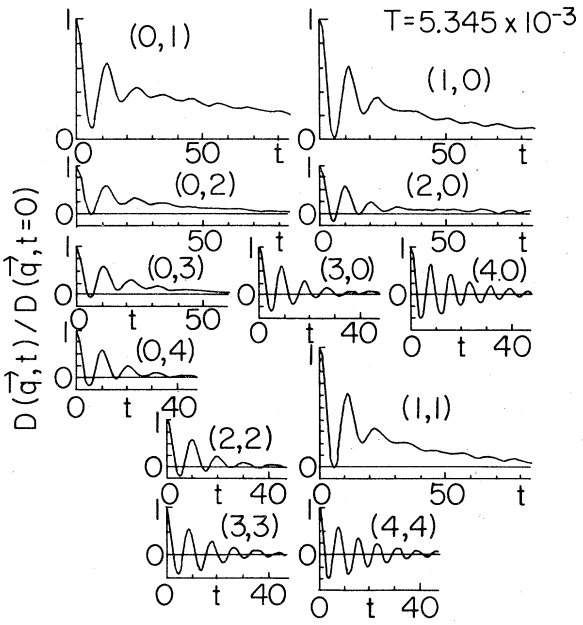

FIG. 26. Time-dependent and wave-vector-dependent correlation function at temperature $T = 5.345 \times 10^{-3}$. The integer pair with each graph identifies the wave vector as described for Fig. 17. Each function is normalized to the value unity at zero time.

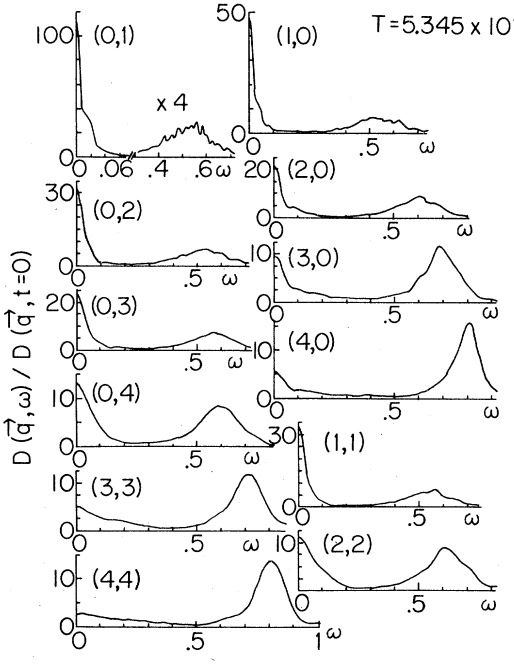

FIG. 27. Spectral functions vs frequency for the normalized wave-vector-dependent displacement correlation functions shown in Fig. 26. The integer pair with each function identifies the wave vector for that function as described for Fig. 17.

a slightly slower decay. This break becomes more pronounced as the temperature decreases and continues increasing as T goes below T_c. At $T=5.798\times10^{-3}$, the rapidly changing part achieves one oscillation before dying out, and at $T=5.345\times10^{-3}$, there is definitely a rapidly varying oscillatory part superimposed on a slowly decaying part. Thus this particular feature of this function behaves in a monotonic fashion through the transition rather than having a singular, more-or-less symmetric behavior about T_c.

In conclusion this section has illustrated the wave-vector dependence of the central-peak characteristics. It has shown that as T approaches T_c, the region of wave-vector space expands where there is a central peak and the central peak becomes more intense throughout this region, and it has shown that there is a smaller region both in wave-vector space and in temperature in which the central peak splits so that the maximum is not exactly at zero frequency.

VIII. ENERGY-DENSITY CORRELATION FUNCTION

The final results to be presented are for the spectral function of the correlation function for the spatial Fourier components of the energy-density fluctuations.

The energy density $h(\vec{R}, t)$ is defined to be that lattice-site dependent quantity whose sum over the lattice is the total energy function H, i.e.,

$$H=\sum_{\vec{R}} h(\vec{R}, t) , \tag{8.1}$$

Since the kinetic energy function and the anharmonic potential-energy function of this model are sums of single-particle terms, their contribution to $h(\vec{R}, t)$ is readily identifiable. The harmonic potential-energy function, given in Eq. (2.5), is a sum of pair terms, so the energy associated with each pair is divided equally between the two particles to obtain the contribution to $h(\vec{R}, t)$. The energy-density function can then be written

$$h(\vec{R}, t)=\tfrac{1}{2}M\dot{v}^2(\vec{R}, t)+\tfrac{1}{4}\{u_0[u_x^2(\vec{R}, t)+u_y^2(\vec{R}, t)]^2+v_0[u_x^4(\vec{R}, t)+u_y^4(\vec{R}, t)]\}$$
$$+\tfrac{1}{4}\sum_{\vec{R}'\alpha\beta}\Gamma_{\alpha\beta}(\vec{R}')[u_\alpha(\vec{R}+\vec{R}')-u_\alpha(\vec{R})][u_\beta(\vec{R}+\vec{R}')-u_\beta(\vec{R})] , \tag{8.2}$$

the last term in this equation being the contribution from the harmonic pair potential. The short range of the forces restricts the sum over $\vec{R}'$ to the nearest and next-nearest neighbors of lattice site $\vec{R}$. The coefficients $\Gamma_{\alpha\beta}(\vec{R}')$ which are nonzero can be identified from Eq. (2.5) and are given in Table I.

The spatial Fourier transform of $h(\vec{R}, t)$ is defined by

$$h(\vec{q}, t)=\sum_{\vec{R}} e^{-i\vec{q}\cdot\vec{R}}h(\vec{R}, t) , \tag{8.3}$$

the correlation function for energy-density fluctuations by

$$E(\vec{q}, t)=N^{-1}\langle h(\vec{q}, t)h(-\vec{q}, 0)\rangle \tag{8.4}$$

and the corresponding spectral function by a temporal Fourier transform, as given in Eq. (7.7) for example.

Since $h(\vec{R}, t)$ is a quadratic and quartic function of the displacements, $E(\vec{q}, t)$ can be considered to be a multiphonon correlation function. That is, if $E(\vec{q}, t)$ were expressed in terms of phonon coordinates, it would contain correlation functions for both two and four phonons, the latter arising from the anharmonic terms in $h(\vec{R}, t)$.

The total energy is a conserved quantity in this model, so $h(\vec{R}, t)$ is a conserved local density. Thus the correlation function $E(\vec{q}, t)$ should exhibit hydrodynamic behavior for small wave vectors. The hydrodynamic limit of $E(\vec{q}, t)$ should have diffusive character, since $h(\vec{R}, t)$ is the only conserved local density of the model.

The results for $E(\vec{q}, \omega)$ from the molecular-dynamics calculations are shown in Figs. 28 and 29. These calculations were done only for temperatures above the transition temperature. Furthermore they were done only for wave vectors near the soft-mode wave vector $\vec{q}_c$, which is the opposite limit from which the hydrodynamic result should apply. Figure 28 shows $E(\vec{q}_c, \omega)$ at wave vector $\vec{q}_c$, for a sequence of temperatures coming down towards T_c. Figure 29 shows $E(\vec{q}, \omega)$ for different wave vectors around $\vec{q}_c$ at $T=6.022\times10^{-3}$, which is the lowest temperature at which these calculations were done and is the temperature at which the soft-mode spectral function shows the most intense central peak. Each of the curves shown in Figs. 28 and 29 has been normalized by the zero time value of the corresponding correlation function, and these initial values are given in Table VI. The pairs of integers labeling the curves in Fig. 29 identify a wave vector $\vec{q}'$, using the same scheme as in Sec. VII, which is the difference wave vector from $\vec{q}_c$ for that particular spectral function.

The results for $E(\vec{q}_c, \omega)$ have a weak central maximum which increases and sharpens only slightly as T decreases to T_c. Around $\omega=0.5$ there is a broad hump in the spectral function which is not very temperature dependent. The most notable change in $E(\vec{q}, \omega)$ is the growth of a well-defined peak at a frequency near $\omega=0.9$. This frequency is considerably higher than the frequencies of any significant spectral weight in the displacement correlations for any of these temperatures.

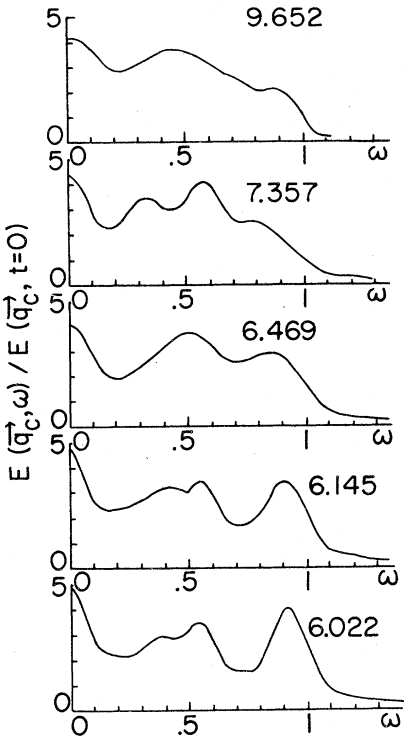

FIG. 28. Spectral function for the energy-density correlation function $E(\vec{q}_c, \omega)$ at the soft-mode wave vector $\vec{q}_c$, as a function of frequency ω, for different temperatures T. The numbers with each curve are the values of $10^3 T$. The curves have all been normalized by the initial value of the correlation function.

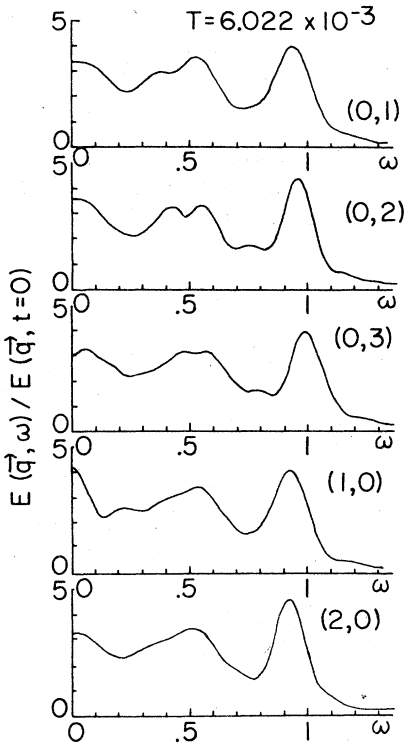

FIG. 29. Spectral function for the energy-density correlation function $E(\vec{q}, \omega)$, at temperature $T = 6.022 \times 10^{-3}$, as a function of frequency ω, for different wave vectors. The integers (m_x, m_y) given with each curve identify a wave vector $\vec{q}' = (2\pi/N_s a)\ (m_x, m_y)$ which specifies the wave vector $\vec{q}$ relative to the soft-mode wave vector $\vec{q}_c$. The curves have all been normalized by the initial value of the correlation function.

TABLE VI. Initial values of the energy correlation function for different temperatures T and wave vectors $\vec{q}$. The wave vector $\vec{q}'$ with integer components identifies the difference between $\vec{q}$ and $\vec{q}_c$ using the same scheme as in Sec. VII.

$10^3 T$	$\vec{q}'$	$E(\vec{q}, t=0)$
9.652	(0,0)	1.831×10^{-4}
7.357	(0,0)	1.175×10^{-4}
6.469	(0,0)	9.206×10^{-5}
6.145	(0,0)	8.447×10^{-5}
6.022	(0,0)	7.908×10^{-5}
6.022	(0,1)	8.025×10^{-5}
6.022	(0,2)	8.121×10^{-5}
6.022	(0,3)	7.885×10^{-5}
6.022	(1,0)	7.756×10^{-5}
6.022	(2,0)	8.022×10^{-5}

These features change as the wave vector $\vec{q}$ changes away from $\vec{q}_c$ as shown in Fig. 29. The intensity of the central maximum in $E(\vec{q}, \omega)$ decreases, and the high-frequency peak increases slightly in intensity. Furthermore, the position of this high-frequency peak exhibits some dispersion, moving to higher frequencies as $|\vec{q} - \vec{q}_c|$ increases.

The high-frequency peak in $E(\vec{q}, \omega)$ presumably demonstrates the existence of a propagating multiphonon resonance in the system, which increases in strength near the transition. The importance of this effect for the nonlinear dynamics is not understood at this time.

IX. CONCLUSIONS

This paper has presented a series of results from molecular-dynamics calculations for a two-dimensional system which exhibits a structural phase transition. The emphasis has been on the dynamical correlations for the order-parameter fluctuations and for the displacement fluctuations for wave vectors around the soft-mode wave vector.

The results for the spectral function for the order-parameter fluctuations show the growth of a very sharp and intense central peak which grows rapidly near the transition, in addition to the soft-mode peak. The temperature dependence found for the soft-mode frequency is the same as has been observed experimentally, for example in $SrTiO_3$. The width of the central peak has been found to follow approximately a square-root temperature dependence for temperatures not too close to the transition. These results depend entirely on the anharmonic character of the potential-energy function of the model, since the model is entirely free of impurities. On the basis of these results the viewpoint is put forward here that the existence of sharp central peaks like those observed in the experiments can be explained on the basis of intrinsic mechanisms inherent in the pure system.

However, it is also clear from experiments, for example that of Hastings *et al.*[33] that impurities do play a role in modifying the dynamical processes that produce the central peak. Further theoretical work is needed to delineate the relative importance and identifying signatures of different impurity effects on the soft-mode dynamics.

Extensive results have also been given here for the spectral functions of the displacement fluctuations for different wave vectors, showing the extent of the wave vector region in which the central peak exists. The central peak has found to split so that the maximum is at a small nonzero frequency, for a small temperature range around T_c and a wave vector region away from $\vec{q}_c$. This result confirms an earlier finding of the same effect by Schneider and Stoll,[40] who have attributed it to propagation of locally ordered clusters. There are no experimental results to date showing this effect so it should still be considered controversial.

Theoretical efforts to explain the central peak based on anharmonic mechanisms have invoked the motion of clusters of locally ordered regions and of the boundaries between these regions. Instantaneous "snapshots" of the atomic displacements patterns during the molecular-dynamics runs show the existence of clusters (these pictures for the present calculations are essentially the same as are shown in Fig. 10 of Ref. 40 so they have not been included here); the same effect is shown by the growth of the static correlation function shown in Fig. 9. However the precise connections of the density of cluster walls, their thickness, and their possible motions to the parameters of the central peak have not yet been made. It is hoped that the results presented here, especially for the wave-vector dependence and for the energy-density correlations will aid in achieving an understanding of these problems.

ACKNOWLEDGMENTS

The author wishes to express his extreme gratitude to Professor Carl Moser for enabling him to spend a year at the Centre Européen de Calcul Atomique et Moléculaire to carry out this work. In addition he is greatly indebted to Dr. Gianni Jacucci for his help in arranging the visit and for greatly increasing the author's knowledge of the physics involved in molecular-dynamics calculations. Dr. Angelo da Fano, Dr. Alexander Tennenbaum, and Dr. Jacucci all provided invaluable assistance in manipulating the CECAM computers. Finally the author wishes to thank Dr. A. Rahman for providing valuable instruction in molecular-dynamics techniques and Professor A. Sjölander for much helpful discussion and correspondence. The part of this research carried out at Wake Forest University was supported by a grant from the Research Corporation.

---

*Permanent address.

[1] *Solitons and Condensed Matter Physics,* edited by A. R. Bishop and T. Schneider (Springer, New York, 1978).

[2] See for example G. Niklasson, Phys. Kondens. Mater. 14, 138 (1972). This is the concluding paper of a series on the theory of weakly anharmonic systems.

[3] W. Cochran, Adv. Phys. 9, 387 (1960).

[4] W. Cochran in *Structural Phase Transitions and Soft Modes,* edited by E. J. Samuelson, E. Anderson, and J. Feder (Universitetsforlaget, Oslo, 1971), p. 1.

[5] P. W. Anderson, in *Fizika Dielektrikov,* edited by G. I. Skanava and K. V. Filippov (Academy of Sciences, Moscow, 1960), p. 290.

[6] G. Shirane and Y. Yamada, Phys. Rev. 177, 858 (1969).

[7] K. A. Müller and W. Berlinger, Phys. Rev. Lett. 26, 13 (1971).

[8] T. Riste, E. J. Samuelson, K. Otnes, and J. Feder, Solid State Commun. 9, 1455 (1975).

[9] S. M. Shapiro, J. D. Axe, G. Shirane, and T. Riste, Phys. Rev. B 6, 4332 (1972).

[10] J. D. Axe, S. M. Shapiro, G. Shirane, and T. Riste, in *Anharmonic Lattices, Structural Transitions and Melting,* edited by T. Riste (Noordhoff, Groningen, 1974), p. 23.

[11] J. K. Kjems, G. Shirane, K. A. Müller, and H. J. Scheel, Phys. Rev. B 8, 1119 (1973).

[12] R. Almairac, M. Rousseau, J. Y. Gesland, J. Nouet, and B. Hennion, J. Phys. (Paris) 38, 94 (1977).

[13] R. A. Cowley, J. D. Axe, M. Iizumi, Phys. Rev. Lett. 36, 806 (1976).

[14] J. D. Axe and G. Shirane, Phys. Rev. B 8, 1965 (1973).

[15] M. D. Mermelstein and H. Z. Cummins, Phys. Rev. B 16, 2177 (1977).

[16] W. D. Ellenson and J. K. Kjems, J. Chem. Phys. 67, 3619 (1977).

[17]K. B. Lyons and P. A. Fleury, Phys. Rev. B 17, 2403 (1978).
[18]K. A. Müller, W. Berlinger, C. H. West, and P. Heller, Phys. Rev. Lett. 32, 160 (1974).
[19]J. Töpler, B. Alefeld, and A. Kollmar, Phys. Lett. A 51, 297 (1975).
[20]S. Aubry, J. Chem. Phys. 62, 3217 (1975).
[21]S. Aubry, J. Chem. Phys. 64, 3392 (1976).
[22]J. A. Krumhansl and J. R. Schrieffer, Phys. Rev. B 11, 3535 (1975).
[23]A. R. Bishop and J. A. Krumhansl, Phys. Rev. B 12, 2824 (1975); A. R. Bishop, E. Domany, and J. A. Krumhansl, Phys. Rev. B 14, 2966 (1977).
[24]P. C. Hohenberg and B. I. Halperin, Rev. Mod. Phys. 49, 435 (1977).
[25]K. G. Wilson and J. Kogut, Phys. Rep. C 12, 75 (1974).
[26]S.-K. Ma, *Modern Theory of Critical Phenomena* (Benjamin, Reading, 1976).
[27]B. I. Halperin, P. C. Hohenberg, and S.-K. Ma, Phys. Rev. B 10, 139 (1974).
[28]R. Bausch and B. I. Halperin, Phys. Rev. B 18, 190 (1978).
[29]See Sec. IV.D.1.b of Ref. 24, and Ref. 28.
[30]B. I. Halperin and C. M. Varma, Phys. Rev. B 14, 4030 (1976).
[31]K.-H. Höck and H. Thomas, Z. Phys. B 27, 267 (1977).
[32]K. A. Müller, N. S. Dalal, and W. Berlinger, Phys. Rev. Lett. 36, 1504 (1976); K. A. Müller and W. Berlinger, Phys. Rev. Lett. 37, 916 (1976).
[33]J. B. Hastings, S. M. Shapiro, and B. C. Frazer, Phys. Rev. Lett. 40, 237 (1978).
[34]T. R. Koehler, A. R. Bishop, J. A. Krumhansl, and J. R. Schrieffer, Solid State Commun. 17, 1515 (1975).
[35]T. Schneider and E. Stoll, Phys. Rev. Lett. 30, 296 (1975).
[36]T. Schneider and E. Stoll, Phys. Rev. Lett. 31, 1254(1973).
[37]T. Schneider and E. Stoll, in *Local Properties at Phase Transitions,* edited by K. A. Müller and A. Rigamonti (Academic, New York, 1977).
[38]T. Schneider and E. Stoll, Phys. Rev. B 10, 4799 (1974).
[39]T. Schneider and E. Stoll, J. Phys. C 8, 283 (1975).
[40]T. Schneider and E. Stoll, Phys. Rev. B 13, 1216 (1976).
[41]M. L. P. Bartolome and W. C. Kerr, Solid State Commun. 21, 253 (1977).
[42]T. Schneider and E. Stoll, Phys. Rev. B 17, 1302 (1978).
[43]The model used for the calculations in Ref. 41 was the same as the model described here except that it had harmonic forces extending out to third-nearest neighbors whose strength was described by two additional parameters r_1 and r_3. These forces did not play an important role so they were omitted from these more extensive calculations. The only consequences were a small decrease in the transition temperature and a weakening of the harmonic forces relative to the anharmonic forces, which was evidenced in the spectral functions by a general increase in the widths of the phonon peaks.
[44]Y. Onodera, Prog. Theor. Phys. 44, 1477 (1970).
[45]A. D. Bruce and A. Aharony, Phys. Rev. B 11, 478 (1975).
[46]H. Thomas, in *Structural Phase Transitions and Soft Modes,* edited by E. J. Samuelson, E. Anderson, and J. Feder (Universitetsforlaget, Oslo, 1971), p. 15.
[47]T. Schneider and E. Stoll, Phys. Rev. Lett. 36, 1501 (1976).
[48]N. D. Mermin and H. Wagner, Phys. Rev. Lett. 17, 1133 (1966).
[49]H. E. Stanley and T. A. Kaplan, Phys. Rev. Lett. 17, 913 (1966).
[50]J. V. José, L. P. Kadanoff, S. Kirkpatrick, and D. R. Nelson, Phys. Rev. B 16, 1217 (1977).
[51]V. G. Makhankov, Phys. Rep. C 35, 1 (1978).
[52]B. J. Alder and T. E. Wainwright, J. Chem. Phys. 33, 1439 (1960).
[53]A. Rahman, Phys. Rev. 136, A405 (1964).
[54]D. Beeman, J. Comput. Phys. 20, 130 (1976).
[55]M. J. L. Sangster and M. Dixon, Adv. Phys. 25, 247 (1976).
[56]L. Verlet, Phys. Rev. 159, 98 (1967); 165, 201 (1968).
[57]These problems have also been discussed in Ref. 40.
[58]G. Gallavoti, Rivista Nuovo Cimento 2, 133 (1977).
[59]Equation (5.1) is different from the corresponding formula in Ref. 40 because the model here has two degrees of freedom per particle, whereas the model of Ref. 40 has one degree of freedom per particle.
[60]J. L. Lebowitz, J. K. Percus, and L. Verlet, Phys. Rev. 153, 250 (1967).
[61]B. M. McCoy and T. T. Wu, *The Two Dimensional Ising Model* (Harvard University, Cambridge, Mass., 1973).
[62]G. Shirane, Rev. Mod. Phys. 46, 437 (1974).
[63]D. R. Nelson and M. E. Fisher, Phys. Rev. B 11, 1030 (1975).
[64]J. M. Kosterlitz, D. R. Nelson, and M. E. Fisher, Phys. Rev. B 13, 412 (1976).